LUT UNIVERSITY
LUT School of Energy Systems
LUT Mechanical Engineering

Otto Ratala

FATIGUE STRENGTH ASSESMENT OF WELDED DETAILS AT WORKSHOP QUALITY

Examiners: Professor Timo Björk
M. Sc. (Tech) Antti Ahola

TIIVISTELMÄ

LUT-Yliopisto
LUT School of Energy Systems
LUT Kone

Konepajavalmistettujen hitsattujen liitosten väsymiskestävyys

Diplomityö

2020

71 sivua, 47 kuvaa, 12 taulukkoa ja 6 liitettä

Tarkastajat: Professori Timo Björk
TkT Antti Ahola

Hakusanat: väsymiskestävyys, nimellinen kuormitus, hot spot, ENS, 4R, lujat teräkset

Tämä työ koostui BW-, LCX- ja LG-hitsien väsymistestauksesta. Nämä hitsit olivat neljän eri yrityksen valmistamia, ja ne testattiin vakiojännitysvaihtelulla. Kappaleet skannattiin erilaisilla menetelmillä (laser, Hexagon ja Winteria), ja saadut skannaustulokset siirrettiin sitten Femap:iin jotta erilaiset tekijät, kuten jännityskonsentraatiotekijät, saatiin määritettyä laskentaa varten.

Koska kappaleissa oli hitsauksen takia kulmavetäymiä, venymäantureita käytettiin näiden muodonmuutosten aiheuttamien taivutusjännitysten määrittämiseen. Kun kappaleita testattiin, niihin oli kiinnitetty venymäantureita, jotka mittasivat kokonaisjännityksen mittausalueelta. Tämän jälkeen Femap-mallit altistettiin puhtaalle kalvojännitykselle, ja taivutusjännityksen määrä voitiin määrittää vertaamalla näitä kahta tulosta.

Sekä nimellis- että hot spot -menetelmät antoivat liioitellun positiivisia tuloksia, mikä osoittaa, että jännityskonsentraatiotekijät ovat välttämättömiä tekijöitä väsymiskestävyydessä, jotka on otettava huomioon, jos halutaan saavuttaa luotettavat väsymiskestävyyden ennusteet. ENS ja 4R suoriutuivat odotettua heikommin, mutta lopulta ENS oli parempi menetelmä koska se tuotti luotettavampia 50 % kestämistodennäköisyystuloksia. Tästä huolimatta 4R näyttää sellaiselta menetelmältä, että se voisi olla parempi näistä kahdesta vaihtoehdosta tulevaisuudessa, koska sen laskenta-arvoja voidaan muokata, mikä näytti vaikuttavan tuloksiin positiivisesti.

ABSTRACT

LUT University
LUT School of Energy Systems
LUT Mechanical Engineering

Otto Ratala

Fatigue Strength of Welded Details at Workshop Quality

Master's Thesis

2020

71 pages, 47 figures, 12 tables and 6 appendices

Examiners: Professor Timo Björk
D. Sc. (Tech) Antti Ahola

Keyworks: fatigue life, nominal stress, hot spot, ENS, 4R, high strength steels

This thesis consisted of fatigue life testing of BW, LCX and LG welds that were produced by four different companies and tested under a constant stress range. The specimens were scanned with various methods (laser, Hexagon and Winteria), and the obtained scanning results were then ported to Femap in order to determine various factors, such as SCFs, that would be used in the calculations.

As the specimens have some angular distortions due to the welding process, strain gauges were used to determine the amount of bending stress that these distortions caused. As the specimens were being tested, they had strain gauges attached to them that would determine the total strain in the measuring area. After this the Femap models would be exposed to pure membrane stress, and by comparing these two differing results, the amount of bending stress could be determined.

Both the nominal and hot spot methods overestimated the fatigue performance results, which indicates that the stress concentration factors are necessary factors to consider if one wants to achieve reliable fatigue life predictions. ENS and 4R performed somewhat below the expectations, but ENS ended up being the better method as it ended up giving more reliable 50 % survival probability results. However, 4R seems like it could be the better method out of the two in the future, as its calculation values can be tweaked, and said tweaking moved the results in a better direction.

ACKNOWLEDGEMENTS

First and foremost, I want to thank the four companies that were a part of this thesis: Mantsinen Group Ltd Oy, Outotec Finland Oy, Wärtsilä Finland Oy and the fourth anonymous one. Without their welding contributions this thesis would have been literally impossible to complete.

Secondly, I want to thank Antti Ahola and Timo Björk for their guidance on the making of this thesis, as well as the staff of LUT Laboratory of Steel Structures who carried out the fatigue testing of the welding specimens and recorded all the necessary measurements. I also want to thank the HRO Design Forum of LUT for funding this research and making it possible.

And finally, I want to express special thanks to professor Harri Eskelinen for all the support and encouragement he has shown me during my bachelor's and master's studies.

Otto Ratala
Lappeenranta 30.10.2020

TABLE OF CONTENTS

TIIVISTELMÄ

ABSTRACT

ACKNOWLEDGEMENTS

TABLE OF CONTENTS

LIST OF SYMBOLS AND ABBREVIATIONS

1 INTRODUCTION 10

2 THEORY 12

2.1 Stress components 12

2.2 Strain gauges 13

2.3 Fatigue strength assessment approaches for welded joints 16

2.3.1 Nominal stress approach 16

2.3.2 Hot-spot stress approach 20

2.3.3 ENS approach 23

2.3.4 4R approach 25

2.4 S-N curves 28

2.5 Quality standard EN ISO 5817 30

3 EXPERIMENTAL TESTING 32

3.1 Specimen preparations 32

3.1.1 Series A 33

3.1.2 Series B 34

3.1.3 Series C 35

3.1.4 Series D 36

3.2 Measurements 37

3.3 Fatigue testing 38

4 NUMERICAL ANALYSIS 41

4.1 Finite element modeling 41

4.2 Point cloud transfer methods 45

4.3 Numerical analysis methods 46

5 RESULTS 51

5.1 Fatigue test results 51

5.2 Numerical analysis results 54

5.3 Quality according to EN ISO 5817 57

6 DISCUSSION 60

6.1 General observations 60

6.2 Suitability of the methods 64

6.3 Limitations and issues 65

6.4 Influencing factors 66

7 CONCLUSIONS 68

LIST OF REFERENCES 70

APPENDIX

Appendix I: Weld toe measurement, part 1.

Appendix II: Weld toe measurement, part 2.

Appendix III: MathCAD-code for solving unknown 4R variables.

Appendix IV: Values used in the calculation of S-N curves, including FAT values at 50 % and 97.7 %.

Appendix V: Test results / calculated values -ratio of the fatigue life results.

Appendix VI: SCFs for ENS and 4R.

LIST OF SYMBOLS AND ABBREVIATIONS

A	Cross-sectional area [mm^2]
b	Variable in S-N curves
b_{ideal}	Ideal plate width [mm]
C	Fatigue capacity
C_{char}	Characteristic curve
C_{mean}	Mean curve
C_{ref}	Reference curve
$C_{ref,char}$	Characteristic reference curve
$C_{ref,mean}$	Mean reference curve
E	Young's modulus [kg/ms^2]
F_{max}	Maximum applied force of test rig [kN]
F_{min}	Minimum applied force of test rig [kN]
f_u	Ultimate tensile strength [MPa]
f_y	Yield strength [MPa]
GF	Gauge factor/stress sensitivity
H	Variable in 4R calculations [MPa]
k	Variable of linear curve in S-N curves
k_2	Variable in S-N curves
k_a	Stress magnification factor at location A
k_b	Bending stress multiplier
k_m	Stress magnification factor
$k_{m,alreadycovered}$	Stress magnification factor already covered in the S-N curve
$k_{m,calculated}$	Stress magnification factor calculated from weld/model
$k_{m,eff}$	Efficient stress magnification factor
k_t	Stress magnification factor of specific weld
$k_{t,b}$	Bending stress magnification factor
$k_{t,m}$	Membrane stress magnification factor
l	Initial length of the conductor [mm]
m	Slope of S-N curve
m_{ref}	Slope of reference curve

N_f	Fatigue life of weld [cycles]
n_{4R}	Variable in 4R calculations
n	Number of test specimens
R	Applied stress ratio
R_{elec}	Initial electrical resistance [Ω]
R_{local}	Local stress ratio present at weld toe
R_m	Material tensile strength [MPa]
r	Weld toe radius [mm]
r_{true}	True weld toe radius [mm]
$Stdv$	Variable in S-N curves
t	Plate thickness [mm]
t_{ideal}	Ideal plate thickness [mm]
x	Variable in S-N curves
y	Variable in S-N curves
Δl	Change in length [mm]
ΔR_{elec}	Change in electrical resistance [Ω]
$\Delta\varepsilon_{meas}$	Measured strain range
$\Delta\sigma$	Stress range [MPa]
$\Delta\sigma_{0.4t}$	Stress range at 0.4t distance from weld toe [MPa]
$\Delta\sigma_{1.0t}$	Stress range at 1.0t distance from weld toe [MPa]
$\Delta\sigma_b$	Bending stress range [MPa]
$\Delta\sigma_{ens}$	ENS stress range [MPa]
$\Delta\sigma_{hs}$	Hot spot stress range [MPa]
$\Delta\sigma_k$	Effective notch stress range [MPa]
$\Delta\sigma_m$	Membrane stress range [MPa]
$\Delta\sigma_{m,calc}$	Calculated membrane stress range [MPa]
$\Delta\sigma_{meas}$	Measured stress range [MPa]
$\Delta\sigma_{nom}$	Nominal stress range [MPa]
β	Weld angle [°]
ε_{1MPa}	Strain of plate under 1 MPa of stress
$\varepsilon_{max,meas}$	Measured maximum strain
$\varepsilon_{min,meas}$	Measured minimum strain

ρ	Resistivity [Ωm]
σ	Stress [MPa]
σ_a	Stress at location A [MPa]
σ_b	Shell bending stress [MPa]
σ_{hs}	Hot spot stress [MPa]
σ_k	Stress at critical peak [MPa]
σ_m	Membrane stress [MPa]
σ_{max}	Maximum stress value of local cyclic behavior [mm]
σ_{min}	Minimum stress value of local cyclic behavior [mm]
σ_{nl}	Non-linear peak stress [MPa]
σ_{res}	Residual stress [MPa]
σ_s	Structural stress [MPa]

BW	Butt Weld
ENS	Effective Notch Stress
FE	Finite Element
FEA	Finite Element Analysis
GMAW	Gas Metal Arc Welding
GTAW	Gas Tungsten Arc Welding
HFMI	High Frequency Mechanical Impact
IIW	International Institute of Welding
LCX	Load-Carrying X-Joint
LG	Longitudinal Gusset Joint
MAG	Metal Active Gas
SCF	Stress Concentration Factor
SDX	Super-Duplex
WPS	Welding Procedure Specification

1 INTRODUCTION

Welding is a common joining method when it concerns plate structures. When a plate structure is under a cyclic stress, the fatigue of the weld joints is a typical form of failure, meaning that the evaluation of fatigue strength is one of the most important forms of design criteria. Generally, the laboratory tests for welded joints are carried out in a controlled environment and the welding itself is either manual, mechanized or robotized, with the quality of the manual workshop welds being less uniform than in mechanized or robotized welding. This disparity of the precise laboratory tests and welding methods against the less precise workshop welding functioned as an inspiration to verify the functionality of the weld toe stress methods for workshop quality welds, and to compare these methods against each other.

With the collaboration of HRO Design Forum, Laboratory of Steel Structures at LUT University worked with four companies (Mantsinen, Outotec, Wärtsilä and one anonymous) to produce various welds that would be fatigue tested and then analyzed with various numerical methods, these being the nominal stress, hot spot, effective notch stress (ENS) and the LUT-developed 4R. LUT prepared and delivered the S700 Plus plates to the companies, after which they could weld their own set with their own instructions and weld types. After this the specimens were measured and fatigue tested in LUT's laboratory, Finite Element Analysis (FEA) was applied to them and the results between different analysis methods were compared. The research questions were set as following:

- Which methods are applicable for fatigue strength assessment of welded details manufactured according to workshop quality?
- What are the factors influencing the fatigue strength capacity in the studied joints?
- Which fatigue-related factors should be determined precisely, and in which case, default or conservative assumptions can be made?

The main limitation of the research was predicted to be the low and limited number of test specimens. For example, the butt-welded A series had only 5 specimens, meaning that if even one of them was faulty, it would notably affect the results. In addition, this is below the minimum number of specimens that various equations use for reliable results, further

limiting the accuracy of the analysis. Only small specimens were tested, meaning that the residual stresses can be smaller than in realistic structures. However, a common joint type which was chosen for welding was a longitudinal attachment, in which the residual stresses are likely to be higher than in the transverse attachment weld joints. Finally, the research is only limited to as-welded joints and the welds were not post-treated.

2 THEORY

Four fatigue strength assessment approaches were used to evaluate the test results of the welded joints in this thesis: nominal stress approach, hot-spot stress approach, ENS concept and the 4R method. In addition, S-N curves based on the fatigue test results were formed based on the so-called Standard approach.

2.1 Stress components

Structural stresses σ_s in plates and shells consist of two parts: membrane stress σ_m and shell bending stress σ_b (Niemi 1995, p. 4). Membrane stress is the average, constant stress that has been calculated through the thickness of the plate. Shell bending stress on the other hand is linearly distributed through the same thickness by drawing a straight line through the intersection of the membrane stress and the mid-plane of the plate. (Hobbacher 2016, p. 13) These stresses are linearly distributed across the plate thickness and are established by FEA based on the theory of shells. Structural stress and its components are presented in figure 1. (Niemi 1995, p. 4)

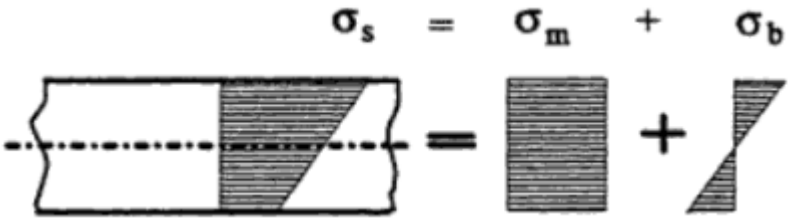

Figure 1. Structural stress and its components (Niemi 1995, p. 4).

The total notch stress on the other hand is made of three components: the previously mentioned membrane stress σ_m, shell bending stress σ_b and a new non-linear peak stress σ_{nl}. Non-linear peak stress is the remaining component of the stress, caused by the local notch. (Hobbacher 2016, p. 14) According to Niemi, it can be separated from the structural stress if a refined stress analysis method that yields a nonlinear distribution across the plate thickness is used. (Niemi 1995, p. 5) Total notch stress and its components are presented in figure 2.

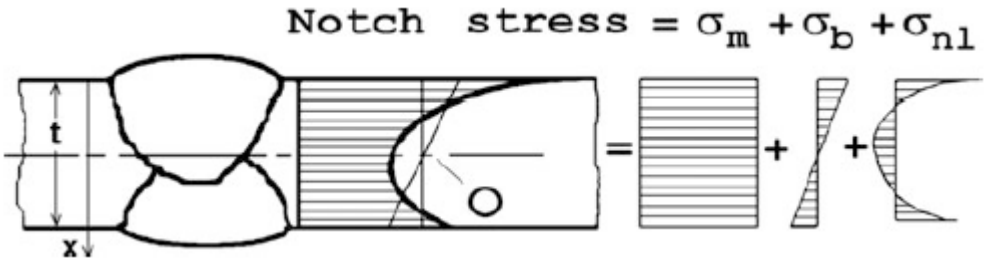

Figure 2. Total notch stress and its components (Hobbacher 2016, p. 14).

2.2 Strain gauges

Strain gauges are small transducers that can be used to measure how much the material elongates when a force affects it. Commonly the strain gauges are small strips that can be attached to the surface of the structure that must be examined. There are five main types of strain gauges: mechanical, hydraulic, electrical resistance, optical and piezoelectric. The mechanical ones consist of two layers, one of which is glued to one side of the elongated/cracked area and one to the other side. One of these layers has a scale and the other has an arrow, and as the crack widens, the arrow moves along the scale. Hydraulic ones amplify the movement of fluid in a gauge, resulting in the detection of small changes in elongation that could go unmeasured with the mechanical gauges. Electrical resistance gauges measure the changing resistance of the gauge, which results from the elongation of material. Optical ones similarly observe the changing optical properties in the gauge, and the piezoelectric gauges are like the electric resistance ones, but instead use ceramics that generate electrical voltages when pushed and pulled. Because only electrical resistance ones were used during the experiments, they are the ones that will be focused on in more detail. (Woodford 2019)

Electrical resistance strain gauges are one of the most widely used strain measurement techniques due to their accuracy, sensitivity, versatility and ease-of-use. Their strain sensitivity is a function of relative electrical resistance change when the conductor is stretched. (Window & Holister 1982, p. 1-3) This means that when the gauge is strained the maze-like wires, as can be seen in figure 3, are either pulled apart or pushed together, which in turn changes the resistance within the gauge. This resistance change can then be converted into a strain. If the deformation is elastic, the gauge returns to the normal as the applied stress decreases, meaning that the measurements can continue over an extended period. (Woodford 2019)

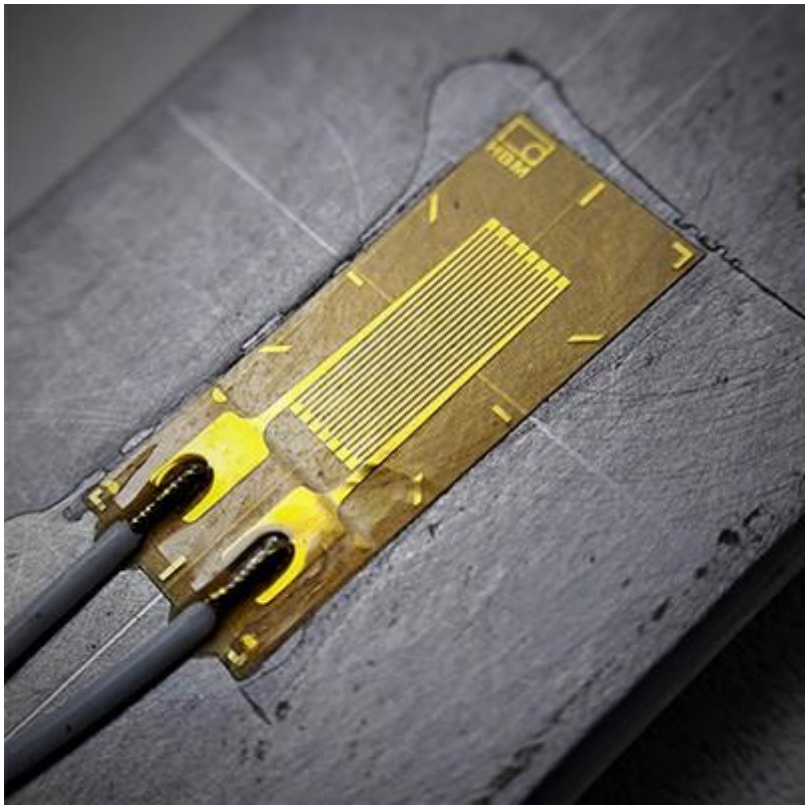

Figure 3. Attached electrical strain gauge (Strain Gauge: Principle, Types, Features and Applications 2019).

As previously mentioned, the gauge's resistance changes during the stress, which can then be converted into strain sensitivity with the help of the changes in length (Window & Holister 1982, p. 3-4):

$$R_{elec} = \frac{\rho l}{A} \quad (1)$$

$$GF = \frac{\Delta R_{elec} \times l}{R_{elec} \times \Delta l} \quad (2)$$

In equation 1 R_{elec} is the initial electrical resistance, ρ is resistivity, l the initial length of the conductor and A is the cross-sectional area. In equation 2 these same meanings apply, while in addition GF stands for gauge factor (also known as strain sensitivity), ΔR_{elec} is the change in electrical resistance and Δl is the change in length. Different electrically conductive materials have their own different gauge factors, established through the effects of geometric changes and resistivity changes. (Window & Holister 1982, p. 3-5) When the other values

are known, these equations can be used to determine the change of length Δl that happens in the strain gauge during the applied stress. This does not require any calculations from the user, as the strain gauge programs determine this on their own.

The strain gauges primarily measure the strain only in the direction of the gauge, and because of this single gauges should only be used when the stress state of the measuring point is known to be uniaxial and the directions of the principal axes are known with reasonable accuracy (±5°). For biaxial stress state two or three element rosette is required. If the directions of principal axes are known, two element 90° rosette can be employed, with the gauge axes aligning with the principal axes. If the principal axes are not known, a three-element rosette must be used, which are available in 45° rectangular and 60° delta configurations. (Window & Holister 1982, p. 34) Before the gauges are placed, the surface area must be cleansed of any organic contamination, oils and greases. Said area should be larger than the gauge, in order to allow for the application of gauge's protective coating and to prevent any possible recontaminations. After degreasing the surface must be brought to the correct degree of surface finish, which depends on the material, type of installation and the adhesive. Things that should be cleaned include any paint, machine marks, mill scale and similar surface imperfections. (Window & Holister 1982, p. 48-50)

When placing the strain gauges, it is also important to correctly place the gauge in relation to any welds or structural discontinuities. As shown in figure 4, both the computed total stress and structural stress increase as a discontinuity is approached. This means that if there are specific placement requirements in regard to the stress concentration locations, like hot spot measuring (or in this thesis, the determination of bending stresses), even a small misplacement can warp the measuring results and falsify the following calculations. To prevent this, the placement of the gauges must be well measured and consistent.

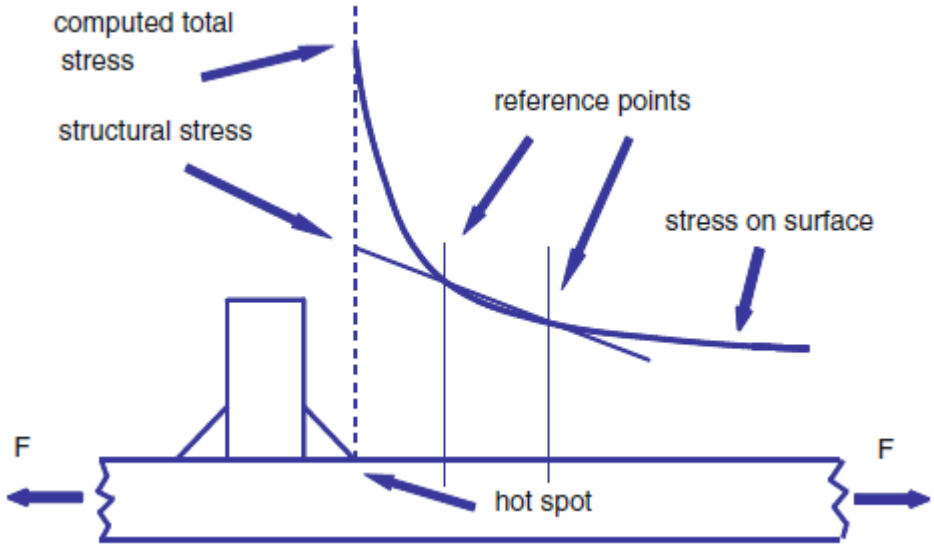

Figure 4. Stress behavior near a welded joint (Hobbacher 2016, p. 19).

2.3 Fatigue strength assessment approaches for welded joints

Following chapters explain the basic idea and the calculations of our four different fatigue strength assessment approaches: nominal stress, hot-spot, ENS and 4R.

2.3.1 Nominal stress approach

Nominal stress approach refers to the stress that is calculated from a chosen area by ignoring the local stress raising effects of the welded joint, while still including the stress raising effects of the macro-geometric shapes, like cutouts, in FAT class. In addition, nominal stress may vary depending on which section is under consideration. (Hobbacher 2016, p. 15) These notch and detail classes are referred to as FAT classes (Radaj, Sonsino & Fricke 2006, p. 20-21), and in S-N curve they have a following relation to the stress range and the fatigue life of the weld (Hobbacher 2016, p. 34):

$$\Delta\sigma^m N_f = FAT^m \times 2 \times 10^6 \quad (3)$$

In equation 3 the $\Delta\sigma$ is the applied stress range to the weld, m is the slope of the S-N curve and N_f is the fatigue life of the weld. Multiple common IIW recommendations for steel structures are presented in the figure 5 along with their FAT values when the survival probability of the weld is 97.7%. Both butt and fillet weld have a varying value that depends on the weld conditions or the dimensions of the welded parts, and the value of cruciform

weld differs based on the location of the failure. Because these welds are used in this research and thus their exact values are important, their conditions are exemplified in figure 6 for the butt weld, in figure 7 for the fillet weld and in figure 8 for cruciform weld. Value of *m* is set to 3 according to the IIW guidelines (Hobbacher 2016, p. 40). In order to acquire the FAT values for 50% survival probability, the FAT value can be multiplied by 1.37. This is because when moving in from a permissible stress amplitude of 97.7% (failure probability of 2.3%) to endurable stress of 50% (failure probability of 50%) as highlighted in figure 9, the amplitude on the vertical axis changes from 0.73 to 1.0, and the ratio of these two values is 1.37. (Radaj et al. 2006, p. 20-22)

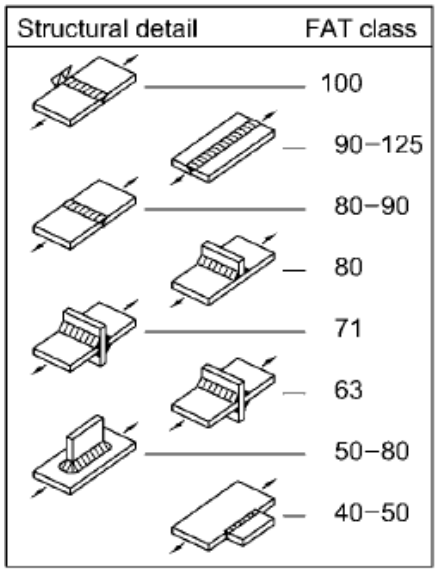

Figure 5. FAT classes for steel at 97.7% survival probability (Radaj et al. 2006, p. 21).

212		Transverse butt weld made in shop in flat position, NDT weld reinforcement <0.1 A thickness	90
213		Transverse butt weld not satisfying conditions of 212, NDT Al.: Butt weld with toe angle ≤ 50° Butt welds with toe angle > 50°	80

Figure 6. Differing conditions for FAT classes in the butt weld (Hobbacher 2016, p. 44)

521		Longitudinal fillet welded gusset of length l. Fillet weld around end l < 50 mm l < 150 mm l < 300 mm l > 300 mm	 80 71 63 50

Figure 7. Differing conditions for FAT classes in the fillet weld (Hobbacher 2016, p. 54).

413	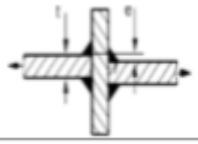	Cruciform joint or T-joint, fillet welds or partial penetration K-butt welds, potential failure from weld toe Single sided T-joints	63 71
414		Cruciform joint or T-joint, fillet welds or partial penetration K-butt welds including toe ground joints, potential failure from weld root For a/t <=1/3	36 40

Figure 8. Differing conditions for FAT classes in cruciform weld (Hobbacher 2016, p. 51).

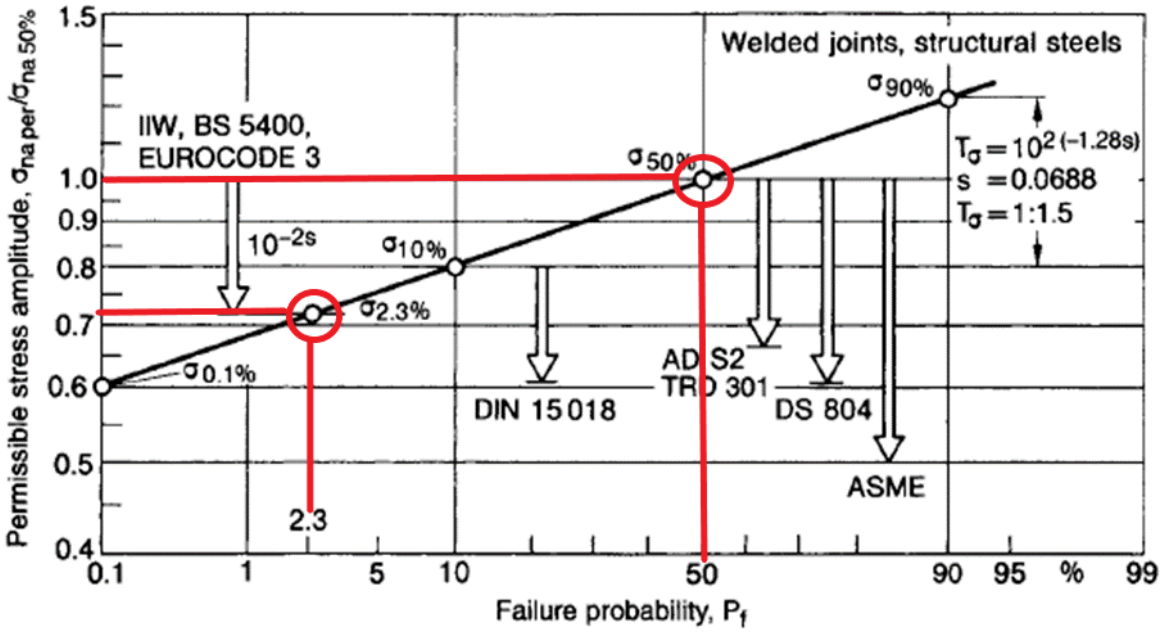

Figure 9. Permissible stress amplitudes derived from endurable stress amplitudes at $2x10^6$ cycles with highlights (Radaj et al. 2006, p. 20).

A finite element method can also be used to calculate the nominal stress. This might be required in situations in which the complex structures are statically over-determined, or the structural components have discontinuities which have no analytical solutions. In these cases, meshing should be simple and coarse. According to the IIW "care must be taken to ensure that all stress concentration effects from the structural detail of the welded joint are excluded when calculating the modified (local) nominal stress". Finally, it should be noted that while nominal stress approach can be used in finite element calculations, more precise options should be considered in its place. (Hobbacher 2016, p. 17)

When under a membrane stress axial or angular misalignments cause secondary bending stress on the structure if they exceed the amount that is covered by the fatigue resistance S-N curve for the structural detail (Hobbacher 2016, p. 15). This bending stress is accounted for by multiplying the membrane stress with an additional stress magnification factor or by calculating the stress via stress analysis. A small amount of misalignment is already included in the fatigue resistance S-N curves, as listed in figure 10. If the listed value is not exceeded, the bending stress multiplier can be ignored. (Hobbacher 2016, p. 80)

Type of k_m analysis	Nominal stress approach	Structural hot spot, effective notch and fracture mechanics appoach	
Type of welded joint	k_m already covered in FAT class	k_m already covered in SN curves	Default value of effective k_m to be considered in stress
Butt joint made in shop in flat position	1.15	1.05	1.10*
Other butt joints	1.30	1.05	1.25*
Cruciform joints	1.45	1.05	1.40*
Fillet welds on one plate surface	1.25	1.05	1.20**
Fillet welds on both plate surfaces	1.25	1.05	1.10***

Figure 10. Consideration of stress magnification factors due to misalignment (Hobbacher 2016, p. 81).

If the stress magnification factor k_m is calculated directly, it can be used in conjunction with the already covered k_m from figure 10 to calculate the efficient stress magnification factor (Hobbacher 2016, p. 81):

$$k_{m,eff} = \frac{k_{m,calculated}}{k_{m,alreadycovered}} \quad (4)$$

In equation 4 $k_{m,\text{calculated}}$ refers to the directly calculated stress magnification factor, while $k_{m,\text{alreadycovered}}$ refers to the values that are already covered in the S-N curve, as presented previously in figure 10 (Hobbacher 2016, p. 81). The IIW presents various formulae for the $k_{m,\text{calculated}}$ values, two of which are presented in figure 11 (Hobbacher 2016, p. 127).

No	Type of misalignment
1	*Axial misalignment between flat plates*
	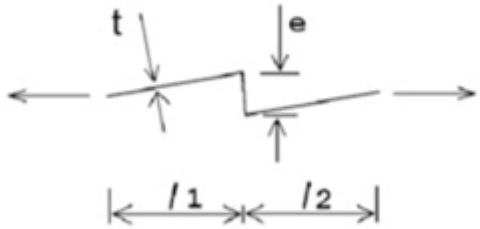 $k_m = 1 + \lambda \cdot \frac{e \cdot l_1}{t \cdot (l_1 + l_2)}$
	λ is dependent on restraint, **λ=6** for unrestrained joints. For remotely loaded joints assume $\mathbf{l_1 = l_2}$.
4	*Angular misalignment between flat plates*
	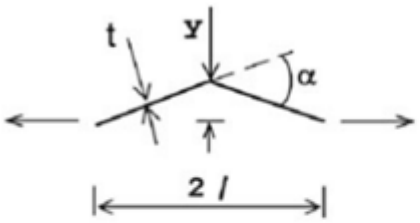 Assuming fixed ends: with $\beta = \frac{2 \cdot l}{t} \cdot \sqrt{\frac{3 \cdot \sigma_m}{E}}$ $k_m = 1 + \frac{3 \cdot y}{t} \cdot \frac{\tanh(\beta/2)}{\beta/2}$ alternat.: $k_m = 1 + \frac{3 \cdot \alpha \cdot l}{2 \cdot t} \cdot \frac{\tanh(\beta/2)}{\beta/2}$ Assuming pinned ends: $k_m = 1 + \frac{6 \cdot y}{t} \cdot \frac{\tanh(\beta)}{\beta}$ alternat.: $k_m - 1 + \frac{3 \cdot \alpha \cdot l}{t} \cdot \frac{\tanh(\beta)}{\beta}$

Figure 11. Examples formulae for $k_{m,\text{calculated}}$ (Hobbacher 2016, p. 127).

2.3.2 Hot-spot stress approach

Structural hot spot stress approach is typically used when the geometry of the joint is too complex or when the structural discontinuity is not comparable to classified structural detail. It is also a more precise method than nominal stress approach, especially if strain gauges are intended to be used. According to Hobbacher (2016) “the structural or geometric stress σ_{hs} at the hot spot includes all tress raising effects of a structural detail excluding that due to the local weld profile itself.” In other words, the non-linear peak stress $\Delta\sigma_{\text{nl}}$ caused by the local notch is excluded, while the global dimensional and loading parameters of the component near the joint are included. Figure 12 exemplifies some structural discontinuities and their corresponding stress distributions. Method is mainly limited to the assessment of weld toes, examples of which are shown in figure 13, but the weld root can also be assessed by using the structural hot spot stress on the surface as an indication of that in the region of interest. (Hobbacher 2016, p. 18-19)

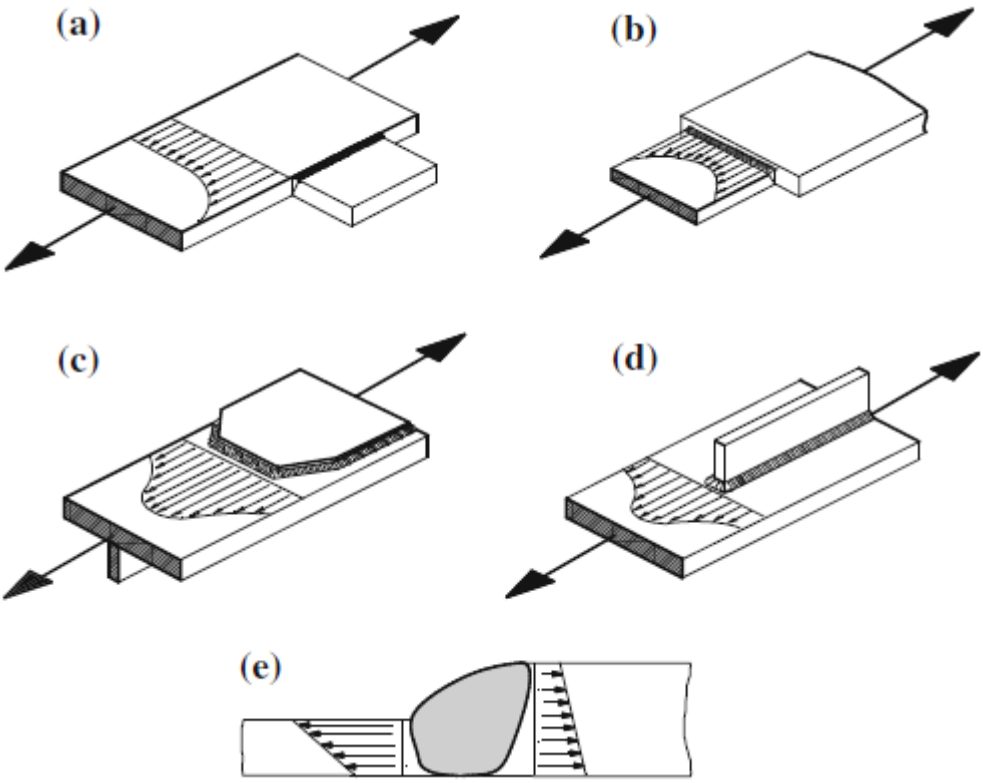

Figure 12. Various structural discontinuities and their stress distributions (Radaj et al. 2006, p. 18).

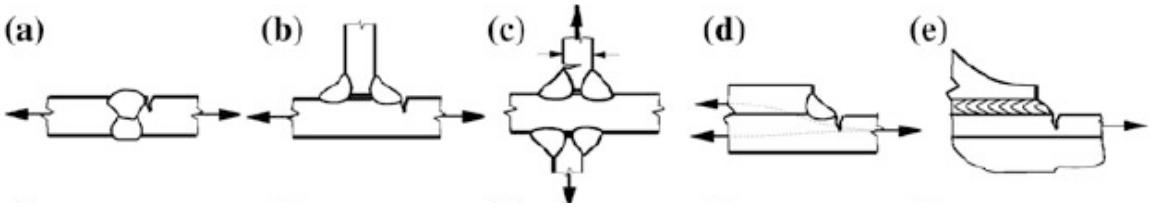

Figure 13. Examples of weld toes that can be reviewed with hot spot method (Radaj et al. 2006, p. 19).

There are two different types of hot spots which are defined based on their location on the plate: either at the weld toe on the plate surface (type a in figure 14) or weld toe at plate edge (type b in figure 14). The type of hot spot determines how the structural hot spot stress σ_{hs} is calculated and which areas need to be referenced for the calculations. In this research, all measured and calculated hot spots were of the type a, and the corresponding reference areas are showcased in figure 15. As shown, these reference points are located at a distance from the weld toe related to the thickness of the plate, with the multipliers being 0.4 and 1.0. As

analytical methods are typically not usable with hot spot method, these values must be determined via FEA. (Radaj et al. 2006, p. 20-23)

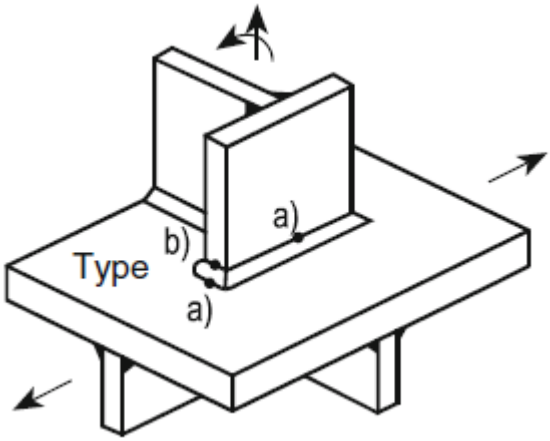

Figure 14. Types of hot spots (Radaj et al. 2006, p. 20).

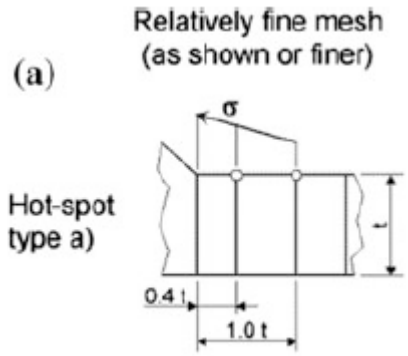

Figure 15. Reference points for fine meshed type a hot spot (Radaj et al. 2006, p. 23).

As established earlier, the welds in this research belong to the type a, meaning that the reference points are located at 0.4*t* and 1.0*t* distances from the weld toe. Using a FEA model the structural stress values can be measured at these points, using both the maximum and minimum loads in order to acquire the hot spot load range (Radaj et al. 2006, p. 23):

$$\Delta\sigma_{hs} = 1.67 \times \Delta\sigma_{0.4t} - 0.67 \times \Delta\sigma_{1.0t} \quad (5)$$

In equation 5 $\Delta\sigma_{0.4t}$ is difference between maximum and minimum stress values at the 0.4*t* reference point in FEA after the structure has been subjected to both maximum and minimum loads, while $\Delta\sigma_{1.0t}$ is the same for the 1.0*t* reference point. After the hot spot range has been

calculated, it can be inserted into the nominal stress equation 3 along with the corresponding FAT value to calculate the fatigue life at 97.7% survival probability. The effects of high tensile residual stresses are included in the FAT, while when it comes to misalignments, only small effects are included (Hobbacher 2016, p. 60). In order to achieve the 50% probability life, FAT can be multiplied with 1.37 as established with the nominal stress earlier.

2.3.3 ENS approach

ENS approach aims to account for both the variation of the weld shape parameters and the non-linear material behavior by replacing the actual weld contour with an effective one. A notch root radius of 1 mm has been verified to give consistent results, and their placement for the welds in presented in figure 16. Note that the root side of the weld is also rounded at the ends of the root gap. This method is not applicable if there is a significant stress component parallel to the weld, if the weld toes and root are not naturally formed as-welded ones or the thickness of the materials is below 5 mm, which requires its own approach. (Radaj et al. 2006, p. 27-28)

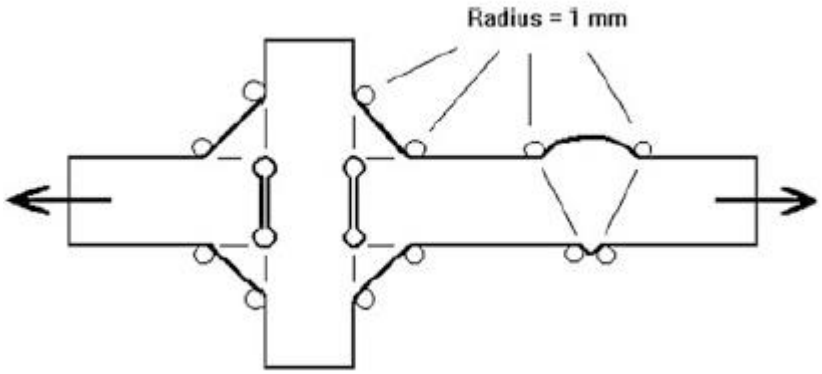

Figure 16. 1 mm ENS rounding of the weld toes and roots (Radaj et al. 2006, p. 27).

Effective notch stresses or stress concentration factors (SCF) can be calculated by parametric formulae, taken from diagrams or calculated by finite element or boundary element models. When using FEA, element size must be at most 1/6 of the radius in the case of linear elements and at most 1/4 of the radius in the case of higher order elements. These sizes must be present both in the curved parts as well as in the beginning of the straight part of the notch surfaces, as presented in figure 17. (Radaj et al. 2006, p. 28-29)

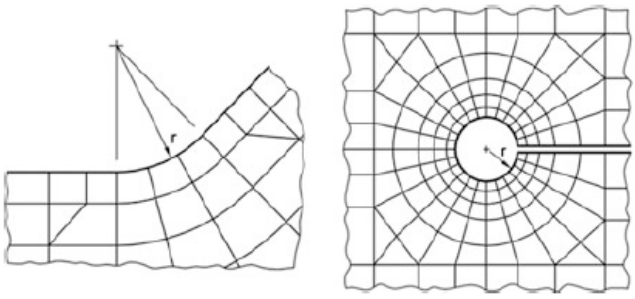

Figure 17. Recommended meshing of the FEA weld toes and roots (Radaj et al. 2006, p. 29).

Finite element programs can be used to determine the membrane and bending stress of the weld (Radaj et al. 2006, p. 33). This can be carried out with the previously mentioned SCFs, which are given for various common discontinuities. SCFs are a ratio of highest stress to reference stress (Carvill 1994):

$$k_a = \frac{\sigma_a}{\sigma} \tag{6}$$

In equation 6 σ_a is the stress at location A, near a discontinuity like a hole, while σ is the normal stress away from any discontinuities. General values for the SCF k_a are usually given for keyways, gear teeth, screw threads and welds. (Carvill 1994) If these references aren't available for any reason, they can be determined from an element model as previously established and, by modifying the equation 6, can be used to determine the stress at a critical peak location if the normal applied stress is known (Gurney 1979, p. 24):

$$\sigma_k = k_t \sigma \tag{7}$$

In equation 7 σ_k is the stress at the critical peak, k_t is the SCF of the specific weld and σ is the applied stress (Gurney 1979, p. 24). If the stress varies with a constant amplitude, the critical stress range can be calculated by replacing the stress values with stress ranges. If the structure is affected by both membrane and bending stress, both of these require their own SCF (Stress Concentration Factors for Shafts and Cylinders 2020), which can then be used together to determine the ENS stress range (Radaj et al. 2006, p. 27):

$$\Delta\sigma_{ens} = k_{t,m}\Delta\sigma_m + k_{t,b}\Delta\sigma_b \tag{8}$$

In equation 8 $k_{t,m}$ and $k_{t,b}$ are the SCFs for the 1 mm weld toe membrane and bending stresses respectively, and $\Delta\sigma_m$ and $\Delta\sigma_b$ are similarly the membrane and bending stress ranges. After the ENS stress range $\Delta\sigma_{\text{ens}}$ has been calculated, it can be placed into the nominal stress equation 3 along with a FAT value of 225 (default in ENS for steel) in order to acquire the fatigue life at 97.7% survival probability. Presented FAT value includes the effects of high residual stresses but does not include the effects of possible misalignment. (Hobbacher 2016, p. 62) The FAT value can once again be multiplied with the previously established 1.37 in order to acquire the results at 50% survival probability.

2.3.4 4R approach

The 4R method is based on the previously mentioned ENS method, and it aims to present an opportunity to consider essential fatigue parameters that are normally not regarded in detail in the calculations. These parameters include material strength, mean stress due to applied load, residual stress from the fabrication processes and real local joint geometry. In order to utilize the 4R method, following material and joint data are needed: material tensile strength R_m, applied stress ratio R, residual stress σ_{res} and weld toe geometrical quality in terms of r_{true}. The method gains its name 4R from the fact of all these four data types having a letter "R" in them. (Björk, Mettänen, Ahola, Lindgren & Terva 2018, p. 1286) According to the material provided by Ahola (2020a) about the process, method is currently applicable for "fatigue assessment of welded joints and cut edges under constant and variable amplitude uniaxial loading", although investigation on multiaxial loads and machine components is currently an ongoing research work.

The 4R method was originally developed by Timo Nykänen, and was initially called the 3R method, as it only included the material tensile strength R_m, applied stress ratio R and residual stress σ_{res}. It is based on existing fatigue test results from literature, and it can be applied for both the as-welded and High Frequency Mechanical Impact (HFMI) treated welded joints. There has also been further testing and development by Heli Mettänen in 2018 in order to make the process applicable for different materials, different joint types/details and post-weld treatments like TIG-dressing. (Ahola 2020a)

The main fatigue life in cycles equation of 4R approach, presented below, resembles the nominal stress/ENS equation on a quick glance, but contains various modifications in order to more accurately account for the weld conditions (Ahola 2020a):

$$N_f = \frac{C_{ref}}{\left(\frac{\Delta\sigma_k}{\sqrt{1-R_{local}}}\right)^{m_{ref}}} \quad (9)$$

In equation 9 the C_{ref} refers to either characteristic reference curve (97.7% survival probability) or mean reference curve (50% survival probability), marked as $C_{\text{ref,char}}$ and $C_{\text{ref,mean}}$ respectively. The numerical values for these are $10^{20.83}$ for characteristic and $10^{21.59}$ for mean. The m_{ref} is the slope of reference curve and is valued 5.85 in both cases. The $\Delta\sigma_k$ is the effective notch stress range and R_{local} is the local stress ratio present at weld toe. While R_{local} requires more work to solve, the $\Delta\sigma_k$ can be calculated relatively easily using the previously established equation 8 (Ahola 2020a). The concentration factors can be solved from a Finite Element (FE) model that uses weld toe radiuses from the following equation (Ahola 2020a):

$$r = r_{true} + 1\ mm \quad (10)$$

In equation 10 r_{true} refers to the original rounding of the physical welded joint. If this is not possible, because there is no requirement for improvement or the rounding cannot be measured, r_{true} is set to 0. R_{local} can be solved from a seemingly simple equation (Ahola 2020a):

$$R_{local} = \frac{\sigma_{min}}{\sigma_{max}} \quad (11)$$

In equation 11 σ_{min} and σ_{max} are the minimum and maximum stress values of local cyclic behavior at weld toe, as presented below in figure 18. However, in order to acquire these values, some work is required. σ_{max} can be acquired by combining the Ramberg-Osgood (R-O) true-stress-true-strain material curve with Neuber's notch theory when it is assumed that the value of strain ε, present in both equations, is equal. (Ahola 2020a):

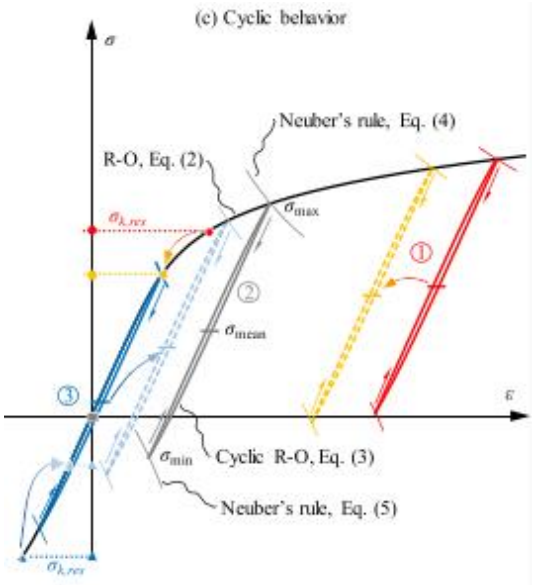

Figure 18. Local cyclic behavior of the weld (Ahola, Skriko & Björk 2019b, p. 6).

$$\frac{\sigma_{max}}{E} + \left(\frac{\sigma_{max}}{H}\right)^{\frac{1}{n_{4R}}} = \frac{(\sigma_k + \sigma_{res})^2}{\sigma_{max} E} \tag{12}$$

In equation 12 the left half is from the R-O theory, while the right half is from the Neuber's theory. E is the Young's modulus, n_{4R} is assumed to have a default value of 0.15 in the 4R method, σ_{res} is the residual stress or equal to the base material's yield strength in the case of as-welded joints (which all our test specimens are when it comes to the breaking area) if the residual stress is unknown, and σ_k can be calculated by using the equation 8 as previously established, but instead of using the stress ranges, only the maximum stress is used. H needs to be calculated by using the base material values (Nykänen & Björk 2015, p. 568):

$$H = 1.65 \times R_m \tag{13}$$

In equation 13 R_m is the base material's ultimate strength. After σ_{max} has been obtained, R-O model and Neuber's theory can again be used to obtain $\Delta\sigma$, which is needed to obtain σ_{min}. However, this time there is a change from a monotonic curve to a cyclic curve, meaning that the equation changes slightly (Ahola 2020a):

$$\frac{\Delta\sigma}{E} + 2\left(\frac{\Delta\sigma}{2H}\right)^{\frac{1}{n_{4R}}} = \frac{{\Delta\sigma_k}^2}{\Delta\sigma E} \tag{14}$$

Once the $\Delta\sigma$ has been solved from the equation 14, it and σ_{max} can be used to solve σ_{min}, finally solving the R_{local} via equation 11 which in turn can be used to solve the 4R fatigue life via equation 9 (Ahola 2020a):

$$\sigma_{min} = \sigma_{max} - \Delta\sigma \tag{15}$$

As previously established with the equation 9, 4R method can produce both the 97.7% and 50% results, eliminating the need for the 1.37 multiplier. It should be noted that while 4R is a reliable method for fatigue failures that initiate from weld toe, in the case of root side fatigue, the verification for the validation of current 4R-version is not conducted.

A slightly steeper slope for the 50 % results was noted in a later research (Ahola et al. 2019b) when compared to the earlier research (Nykänen 2016). The values from this later research were used in addition to the previously established ones in order to compare them. The new calculations were otherwise the same, except $C_{ref,mean}$ was set to be $10^{18.27}$ and m to be 4.65 instead of the previously established values. (Ahola et al. 2019b, p. 9)

2.4 S-N curves

The S-N curves were calculated and drawn based on the so-called "Standard procedure" as the method is known among the professionals (Ahola 2020b). In it the fatigue life is a dependent variable, and the stress range is an independent variable, meaning that only the fatigue life deviation is considered in relation to the estimated curve. It resembles the fatigue resistance determination of the IIW Recommendations (Hobbacher 2016, p. 75-78), but for this research the calculations were based on the teaching material of LUT. The fatigue test results (stress range $\Delta\sigma$ and fatigue life N_f) are plotted in a log-log coordinate system, forming a linear curve (Ahola, Björk & Skriko 2019a, p. 5-6):

$$y = kx + b \tag{16}$$

In equation 16 the variables y, x, k and b stand for various other values, most of them being log conversions (Ahola et al. 2019a, p. 6):

$$y_i = \log N_{f,i} \tag{17}$$

$$x_i = \log \Delta\sigma_i \quad (18)$$

$$k = -m \quad (19)$$

$$b = \log C \quad (20)$$

In equation 19 *k* stands for a variable of the linear curve, while *m* is the slope of S-N curve. Similarly, in equation 20 *b* is another variable of the S-N curve, while *C* is the fatigue capacity presented below, along with alternative calculation methods for variables *k* and *b* utilizing equations 17 and 18 (Ahola et al. 2019a, p. 5-7):

$$C = FAT^m * 2 * 10^6 = \Delta\sigma^m N_f \quad (21)$$

$$k = \frac{n\sum_{i=1}^{n} x_i y_i - \sum_{i=1}^{n} x_i \sum_{i=1}^{n} y_i}{n\sum_{i=1}^{n} {x_i}^2 - \left(\sum_{i=1}^{n} x_i\right)^2} \quad (22)$$

$$b = \frac{\sum_{i=1}^{n} y_i}{n} - k\frac{\sum_{i=1}^{n} x_i}{n} \quad (23)$$

In equations 22 and 23 *n* stands for the number of test specimens. It should be noted that if the said number is below 10, fixed slope is used, resulting in *m* gaining a value of 3 (and thus *k* gaining the value of -3 due to equation 19), meaning that only *b* (equation 23) needs to be calculated. If the weld details are assessed based on shear stress, the *m* value can instead be replaced with 5 (and thus *k* gains the value of -5) (Hobbacher 2016, p 40). After this the mean fatigue strength of all specimens at 2 million cycles ($2*10^6$), representing 50% survival probability, can be calculated (Ahola et al. 2019a, p. 7-8):

$$FAT_{50\%} = \sqrt[-k]{\frac{10^b}{2*10^6}} = \sqrt[m]{\frac{C}{2*10^6}} \quad (24)$$

In order to acquire the 97.7% survival probability FAT, some additional calculations are required. First, a new k_2 value is needed (not to be confused by the previous *k*). This has its own equation, which has been used to calculate values needed for this research that are presented in table 1 (Ahola et al. 2019a, p. 9):

$$k_2 = 1.645 \times \left(1 + \frac{1}{\sqrt{n}}\right) \quad (25)$$

Table 1. k_2 values calculated with equation 25.

n	4	5	8	16
k	2.47	2.38	2.23	2.06

After this, the FAT value for 97.7% survival probability can be determined with the help of the standard deviation (Ahola et al. 2019a, p. 9):

$$C_i = \Delta\sigma_i{}^m N_{f,i} \tag{26}$$

$$Stdv = \sqrt{\frac{\sum_{i=1}^{n}(\log C_{mean} - \log C_i)^2}{n-1}} \tag{27}$$

$$\log C_{char} = \log C_{mean} - k \times Stdv \tag{28}$$

$$FAT_{97.7\%} = \sqrt[m]{\frac{C_{char}}{2*10^6}} \tag{29}$$

With these calculated values the 50% and 97.7% survival probability curves can be plotted into the S-N curve, with the stress range $\Delta\sigma$ at vertical axis and fatigue life N_f at horizontal axis. After this the values of the test results can also be plotted into the same curve as singular dots.

2.5 Quality standard EN ISO 5817

The EN ISO 5817:2014 standard covers the quality levels for imperfections in fusion-welded joints in steel, nickel titanium and their alloys, and it contains a simplified selection of fusion weld imperfections based on the ISO 6520-1. The standard lists a variety of welding imperfections that are commonly present in normal fabrication welding joints, as well as the parameters that are required to achieve one of the three quality ranks: B, C or D. It should be noted that the quality levels provided are just basic reference data and do not specifically relate to any specific application. Normally it is expected that the dimensional limits for imperfection of a welded joint could all be covered by specifying one quality level. However, in some cases it may be necessary to specify different quality levels for different imperfections in the same welded joint. (ISO 5817 2014, p. 11)

Out of all the imperfections listed in the EN ISO 5817 (2014 p. 17-32), those that could be applied to the tested joints were picked and then used to qualify the imperfections. The

chosen imperfections and which welds they were used for are listed below in table 2. The review of the welds was performed based on the FEA as the physical specimens were unavailable at the time of the review and as such a couple of the imperfections regarding weld penetrations were left out as there was no sure way to determine them from the models.

Table 2. Chosen welding imperfections and their applications, categorized by weld joint type: butt weld (BW), longitudinal gusset joint (LG) and load-carrying X-joint (LCX).

No.	Designation	BW joints	LG joints	LCX joints
1.6	Incomplete root penetration	X		
1.7	Intermittent undercut	X	X	X
1.9	Excess weld metal (butt)	X		
1.10	Excessive convexity		X	X
1.11	Excess penetration (butt)	X		
1.12	Incorrect weld toe angle	X	X	X
1.14	Sagging (butt)	X		
1.16	Excessive asymmetry of weld		X	X
1.17	Root concavity (butt)	X		
1.20	Insufficient throat thickness		X	X
1.21	Excessive throat thickness		X	X
3.1	Linear misalignment (butt)	X		

3 EXPERIMENTAL TESTING

Testing of the fatigue specimens required proper preparations and measurements beforehand. This chapter covers all of these.

3.1 Specimen preparations

The plates used in the fatigue testing were originally laser cut to their final shape and then ground in order to remove any sharp edges or remaining minor imperfections. The thickness of the specimens varied between 8 mm and 12 mm, with the specific values for each series being mentioned below in the corresponding figures. Figure 19 illustrates the dimensions of the LG plates for specimens B5-8, C5-8 and D1-8. The letters A, B, C and D refer to the four companies who took part in this thesis, although which specific ones out of the four they refer to is classified. These same dimensions were also used for the butt welds in specimens A1-5, apart from removing the middle plate and cutting the larger main plate in half at the middle. Figures 20 and 21 illustrate the dimensions of the LCX plates for specimens B1-4 in the case of figure 20 and specimens C1-4 in the case of figure 21.

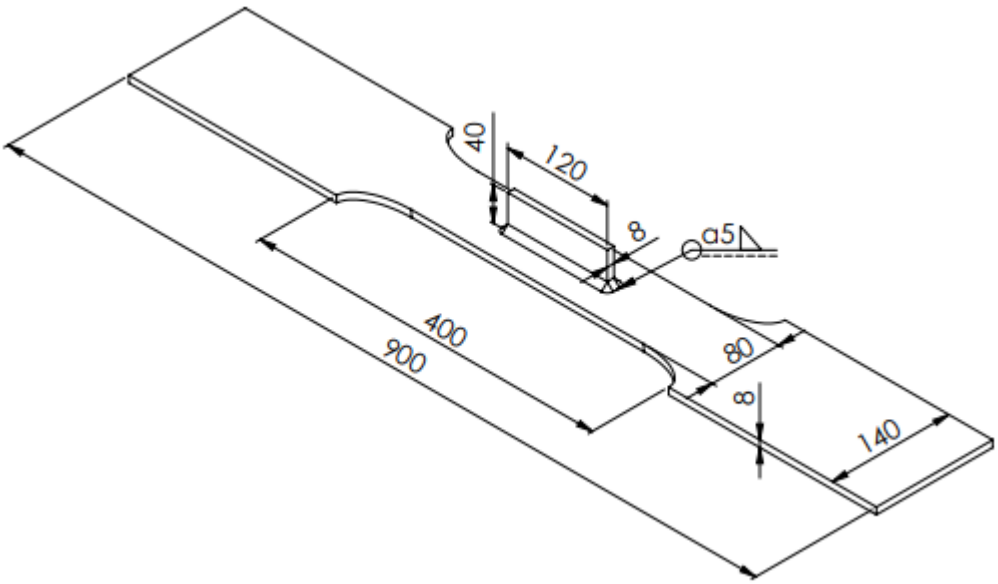

Figure 19. Dimensions of the LG welded plates for specimens B5-8, C5-8 and D1-8.

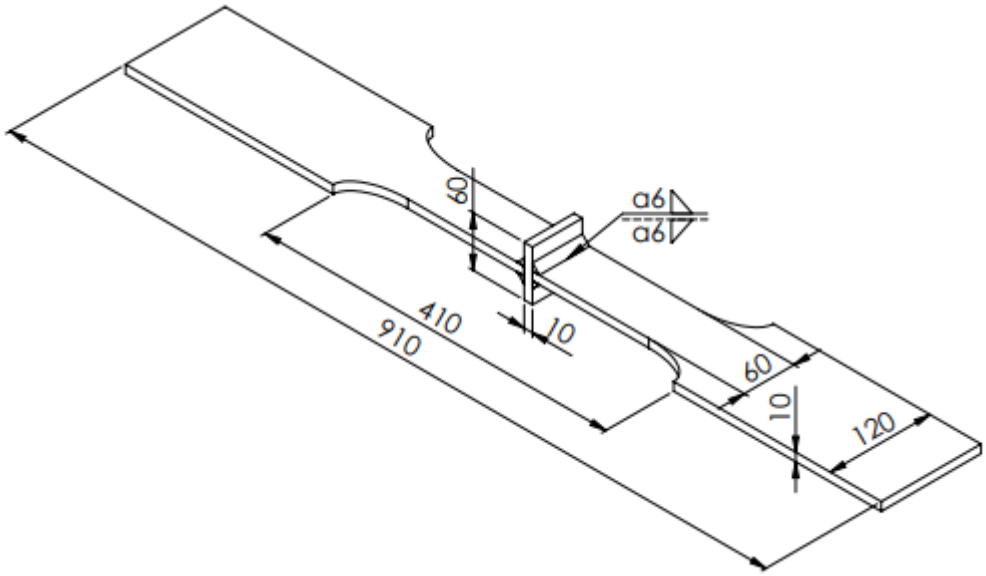

Figure 20. Dimensions of the LCX welded plates for specimens B1-4.

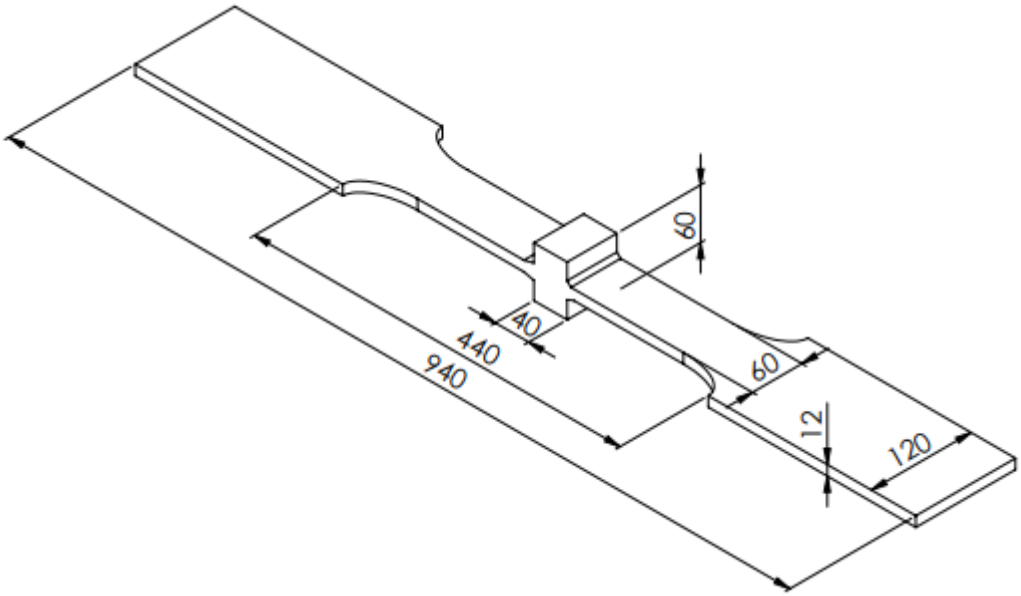

Figure 21. Dimensions of the LCX welded plates for specimens C1-4.

3.1.1 Series A

Series A consisted of 5 dissimilar butt-welded joints with Strenx 700MC and Strenx 900MC base materials, an example of which is presented in figure 22. The joints were welded with a single gas tungsten arc welding (GTAW) pass, with specimens A1-A3 using AristoRod 12.50 as their filler material, while A4-A5 used AristoRod 69. The plates had a thickness of 8 mm and a width of 60 mm.

Figure 22. Close up of series A specimen 4 with a strain gauge.

3.1.2 Series B

Series B consisted of two sets of welds: B1-B4 which were LCX joints as shown in figure 23 and B5-B8 which were LG joints. B1-B4 used plates made from S235 steel, while B5-B8 used plates made from S700MC Plus steel. The LCX joints were welded using gas metal arc welding (GMAW) process, with the welding order exemplified in figure 24. The welding areas were originally widened so that the starting and finishing areas of the welding process could be removed from the specimen. This milling was carried out bit by bit in order to avoid any deformations on the specimens. Esab AristoRod 12.50 was used as a filler material for both sets. The attached middle part was 10 mm thick in B1-B4 LCX cases, and 8 mm in B5-B8 LG cases, which is also the thickness for the main plates in both cases. The width of the B1-B4 specimens was 60 mm and 80 mm for the B5-B8 specimens.

Figure 23. Series B specimen 1 with strain gauges attached.

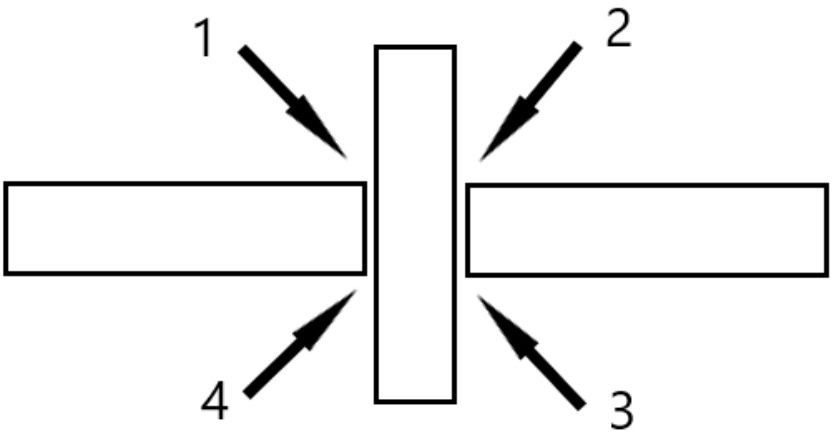

Figure 24. LCX welding order of series B specimens 1-4.

In the case of specimens B5-B8, shown in figure 25, welding was carried out with two GMAW passes: first the one end of the attachment was welded, starting from the middle of the longitudinal side, moving on to the end and continuing the middle of the other longitudinal side. The second weld was a repeated version of this weld. This process is also demonstrated in figure 25 and was carried out in order to avoid any distortions of the crack location at the end of the fillet due to the starting/ending location of welding.

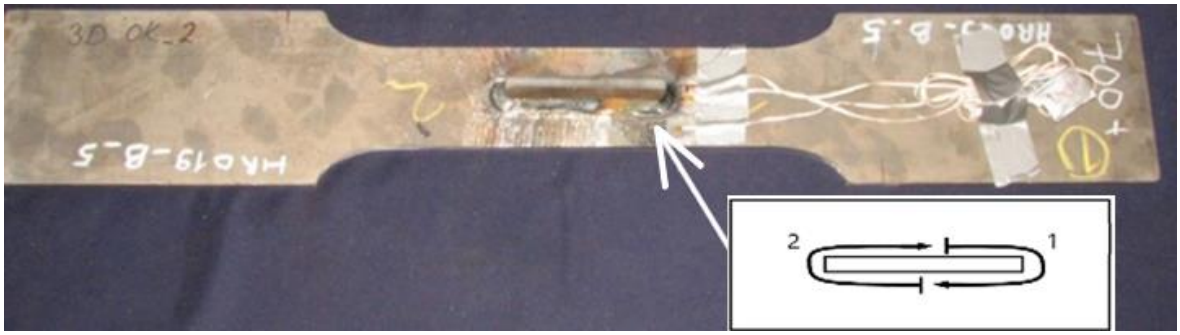

Figure 25. Series B specimen 5 with strain gauges attached, and the welding sequence.

3.1.3 Series C

Series C also consisted of two welding sets: specimens C1-C4 were again LCX welds as shown in figure 26 while the specimens C5-C8 were LG welds, carried out the same way as established previously. AristoRod 12.50 was again used as the filler material and the welding method was similarly GMAW as in series B. Specimens C1-C4 used S355 plates with a thickness of 12 mm and width of 60 mm, with the middle section between the plates being

40 mm thick, while the specimens C5-C8 used the S700MC Plus steel with the default 8 mm thickness and 80 mm width.

Figure 26. Series C specimen 1 with strain gauges attached.

3.1.4 Series D

Series D was also made of two sets of welds, however this time both D1-D4 and D5-D8 sets were LG welds as shown in figure 27. Welds D1-D4 had EN 1.4410 as base material and Avesta 2507 as filler material, while the D5-D8 welds had S700MC+ as base material and Esab OK Tubrod 14.03 as filler material. Welding method for the D1-D4 set was GMAW and the D5-D8 set used metal active gas (MAG) welding. Both sets had a plate thickness of 8 mm and width of 80 mm.

Figure 27. Series D specimen 5 with strain gauges.

During the welding process both sets also had a small, 3 mm support plates underneath the middle of the specimens with clamps at the ends in order to create pre-welding bending to counteract the bending deformations in the other direction caused by the welding.

Table 3 contains a summary of the previously mentioned information, listing the joint types, base materials and filler materials. Both the base and filler materials also have their yield strength f_y and ultimate tensile strength f_u listed.

Table 3. Summary of the weld types, base materials and filler materials.

Company	ID	Joint	Base material			Filler material		
			ID	f_y [MPa]	f_u [MPa]	ID	f_y [MPa]	f_u [MPa]
A	A_1-3	BW	S700MC	700	750-950	AristoRod 12.50	430	530
			S900MC	900	930-1200			
	A_4-5	BW	S700MC	700	750-930	AristoRod 69	730	800
			S900MC	900	930-1200			
B/C	B_1-4	LCX	S235	235	360	AristoRod 12.50	430	530
	C_1-4	LCX	S355	355	430	AristoRod 12.50	430	530
B/C/D	B_5-8	LG	S700MC+	700	750-950	AristoRod 12.50	430	530
	C_5-8	LG	S700MC+	700	750-950	AristoRod 12.50	430	530
	D_1-4	LG	SDX 2507	550	750-1000	Avesta 2507	660	860
	D_5-8	LG	S700MC+	700	750-950	OK Tubrod 14.03	757	842

3.2 Measurements

Welds of the series A were measured via a laser measurer, as the series was scheduled for testing while more accurate machinery was in maintenance. The laser moved a 50 mm long distance along the middle of the side (both sides were measured), with the middle point of this movement being the weld, as shown in figure 28. These results were compiled into a point cloud for later FE modeling.

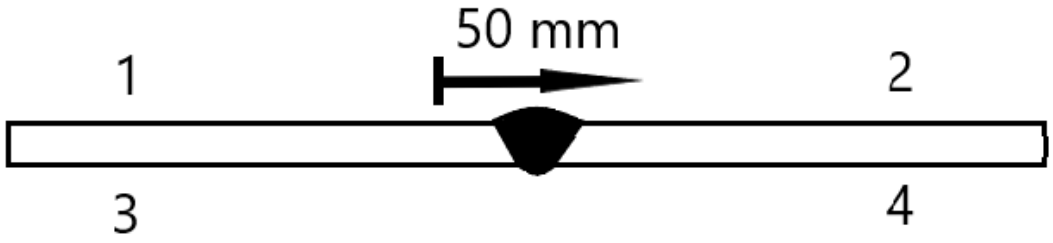

Figure 28. Draft for the laser scanning of series A.

The LG welds were measured using a Hexagon-branded laser scanner, which forms a 3D image as shown in figure 29. With this method, there were two available precisions: 1.0 mm and 0.5 mm. Originally the specimens were first scanned with the 1.0 mm precision and the weld area was afterwards specifically scanned with the 0.5 mm precision. The idea was that this way the model's file size would remain manageable while the weld itself would still be recorded with enough accuracy. Later it was found out that the scanner did not overwrite any sections measured with the 1.0 mm accuracy with the 0.5 mm one, meaning that some

of the welds were recorded with smaller accuracy. After this the rest of the specimens were scanned only with the 0.5 mm accuracy, but few specimens had already been tested and thus could not be rescanned.

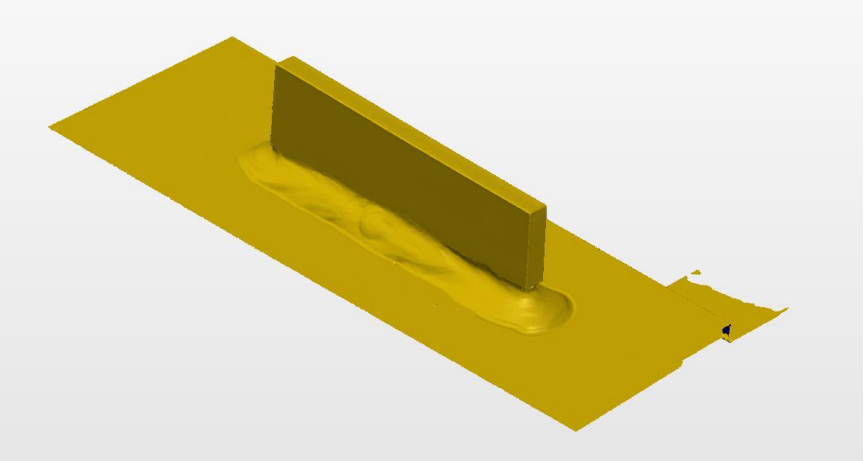

Figure 29. Hexagon 3D model of Series B specimen 5.

The LCX welds were measured with Winteria-branded scanner. Instead of forming an interactive 3D model, the scanner instead moves along the weld, scanning multiple "slices" one after another, listing the outline of the weld as point cloud, as well as recording the weld toe radiuses and weld toe angles for each "slice". The program can record a lot of additional information, including if said information is within acceptable limits, but the previously listed info was what was needed for the upcoming research steps.

The combined measurements for all the specimens are presented in appendices I and II. Appendix I consists of weld types, materials, *a*-measurement of the weld and the weld toes' *r*-measurements. Appendix II in turn consists of stress ratio *R*, calculated membrane and bending stress ranges $\Delta\sigma$, angular error between the attached plates and the weld angle β. In the case of BW and LCX welds all weld toes were measured (BW welds used the same numbering order as in figure 24), while in the case of LG welds only the toe that ended up failing was measured.

3.3 Fatigue testing

Fatigue testing was carried out via two fatigue test rigs, one with the maximum force capacity of 750 kN and the other with the maximum force capacity of 1200 kN. Majority of the tests

were carried out utilizing the 1200 kN test rig. Before the actual testing was started, strain gages were attached to the specimens, either at 0.4*t* and/or 1.0*t* distance from the weld along the middle of the specimen, and/or 15 mm from the outer edge of the specimen along the weld in order to determine the bending portion of the total stress with the help of FEA and the strain gauges. The differences result from the different requirements that the different joints possess: transverse welds lack a stress concentration, meaning that one gauge at 0.4*t* distance is enough. Longitudinal welds however have a concentration, meaning that more gauges are required. The summary of these gauge placements is presented in table 4. After the attachment, the strain gages were calibrated with a handful (1-5) of static stress cycles.

Table 4. Strain gauge attachments for different weld sets.

	0.4 *t*	1.0 *t*	15 mm from edge
Series A, 1–5	X		
Series B, 1–4	X		
Series B, 5–8	X	X	X
Series C, 1–4	X		
Series C, 5–8	X	X	X
Series D, 1–4	X		
Series D, 5–8	X	X	X

Series B, C and latter half of D (5-8) also had one side of their LG welds peened with HFMI treatment, as shown in figure 30. This was performed in order to force the specimens to fail from the weld toe in the as-welded condition, which in turn allowed for the strain gages to be attached to the correct side without any guessing. This was not carried out for the series D specimens 1-4, because they were made from Super-Duplex (SDX) 2507 steel grade. LUT has previously noticed that HFMI-treating this metal might cause micro crack initiation in the specimens, thus distorting the test results (Björk et al. 2018, p. 1299–1300). The remaining BW and LCX welds did not receive any kind of corresponding post-weld treatments.

Figure 30. HFMI-treated weld toe of series B specimen 5.

The stress range was kept the same during the actual dynamic fatigue testing process, with the stress ratio R being either 0.1 or 0.5. This also means that both the maximum and minimum applied force of the test rigs F_{max} and F_{min} were positive and above zero during the whole testing process in all the cases. The loading rate of the tests varied between 1-2 Hz. During testing the output of strain gages in relation to amount of cycles was tracked and recorded.

4 NUMERICAL ANALYSIS

Majority of the fatigue life calculations required values that in our case could only be acquired via FEA. This chapter covers the necessary steps that were taken in order to acquire these values.

4.1 Finite element modeling

In order to acquire hot spot stresses and notch SCFs needed for the analysis, FE-models for the joints needed to be constructed. This was executed by transferring the scanned/measured 2D joint geometry into Femap as a point cloud representing the outline of the weld, as shown in figure 31, and then modeling a quarter model joint based on this information, by first forming the outlines of the model with curves and plate elements and then extruding them into solid elements, as shown in figures 32 and 33. Figure 32 also showcases how the area around the weld toe had additional smaller sections which would have a smaller element size than the rest of the model. While rest of the model near the weld had an element size of 0.5 mm, these areas would have an element size of 0.05 mm in order to provide more accurate results for the calculations. In other locations of the model there were no such specific requirements for the element sizes.

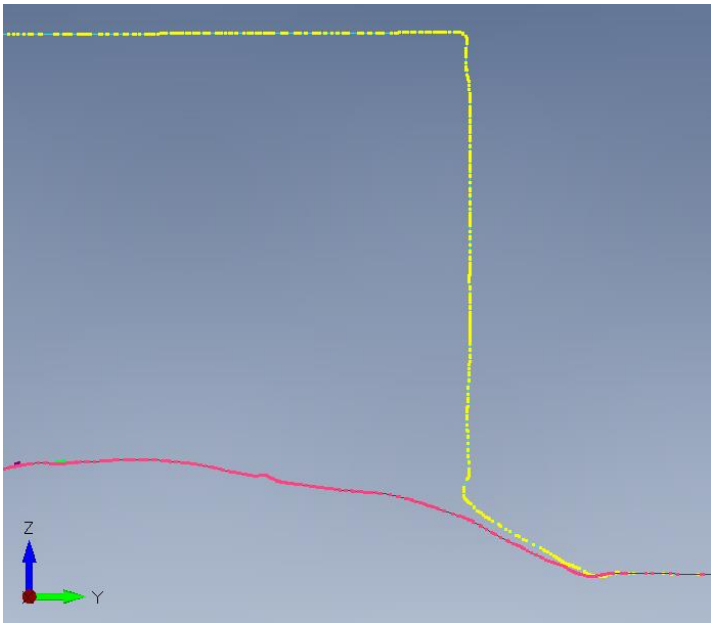

Figure 31. Transferred point cloud of a LG weld in Femap.

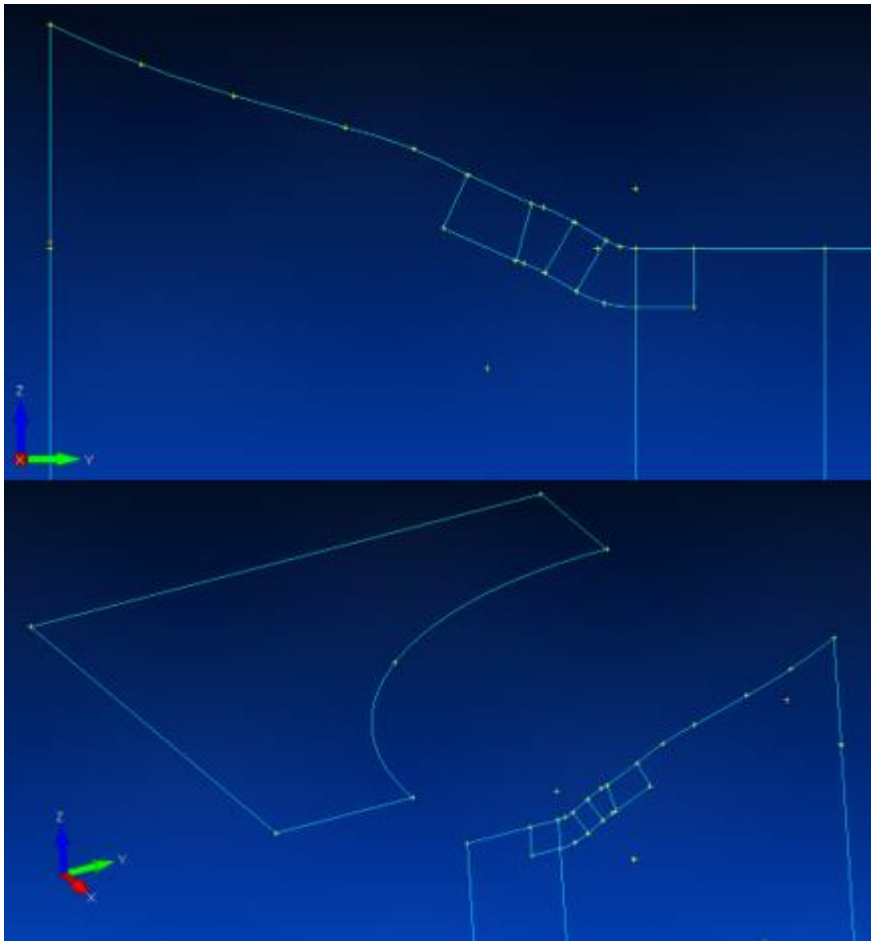

Figure 32. LG weld's modeled curves in Femap.

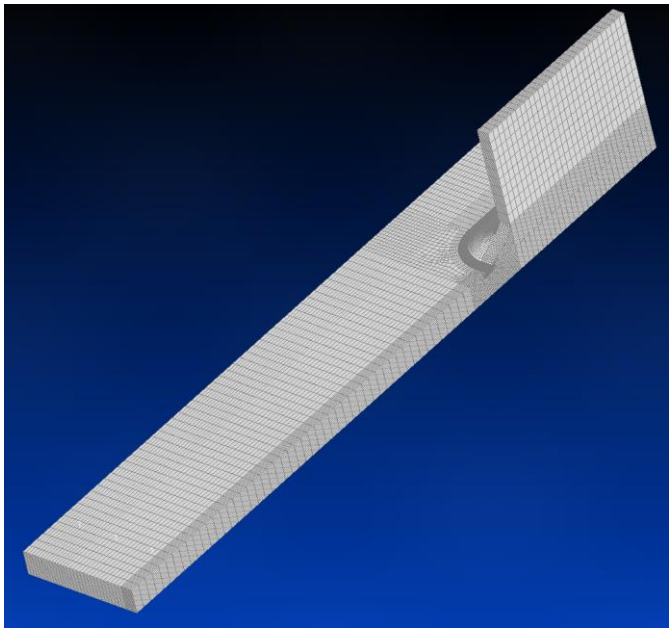

Figure 33. Finished quarter model of the LG joint in Femap.

While hard to see, there is also a small 0.1 mm gap between the bottom plate and the attachment as shown in figures 34 and 35, meaning that they are connected to each other only by the weld. The models were also constructed in such a way that there would be an element border at 0.4*t* and 1.0*t* distance from the weld toe in order to get accurate results from these specific locations, as showcased in figure 36 with the two lowest horizontal lines.

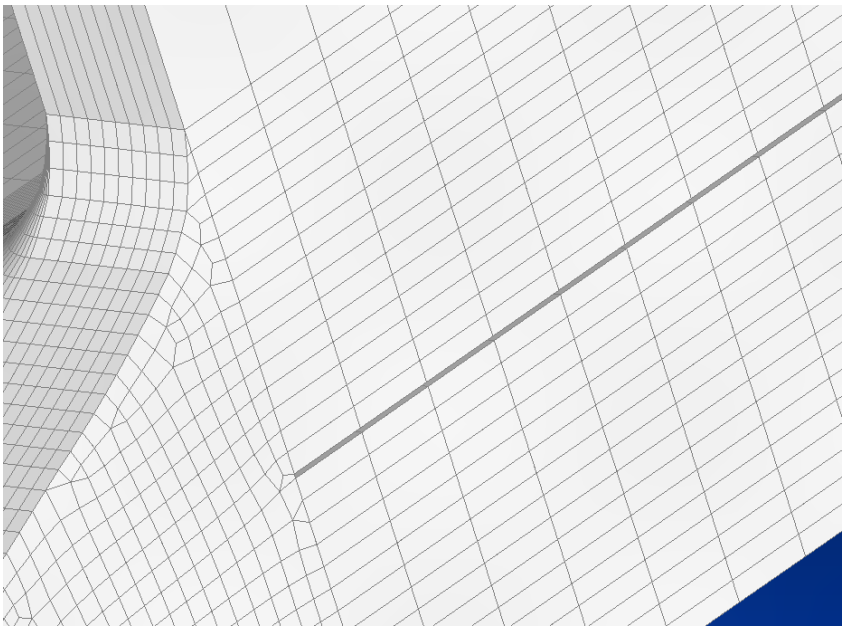

Figure 34. 0.1 mm gap between the welded parts LG weld.

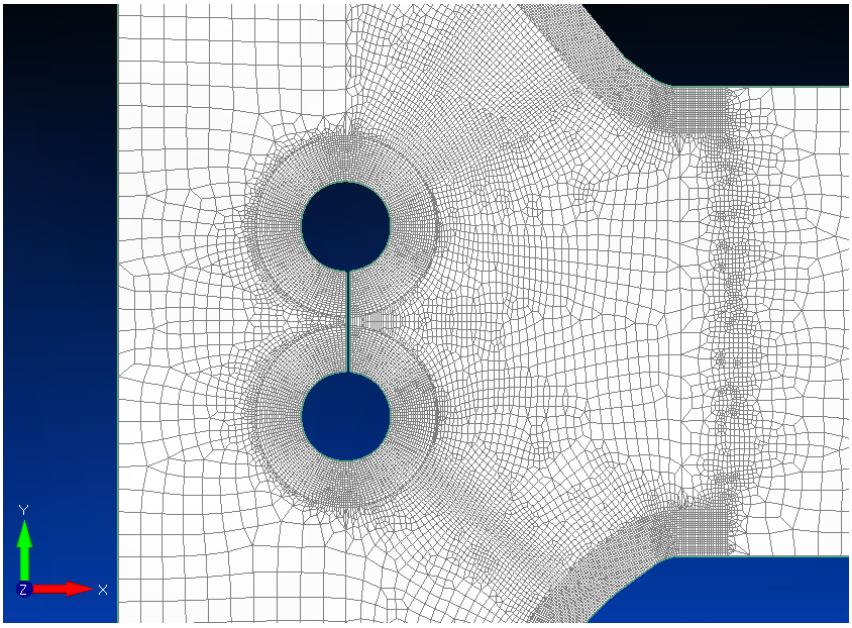

Figure 35. 0.1 mm gap between the welded parts in LCX weld.

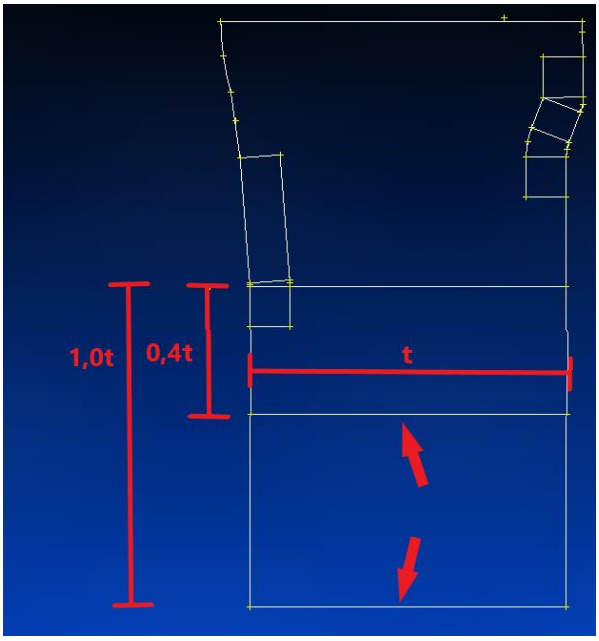

Figure 36. 0.4t and 1.0t element borders of BW weld, highlighted with arrows.

The material used in these models used Young's modulus of 210000 MPa and a Poisson's ratio of 0.3. The stresses were applied to the surface at the end of the model as a Force Per Area. For the membrane stress a constant value that was the same on the whole end was given, and for the bending stress a formula for a varied stress was given. This formula, dependent on the model's height axis, would give the stress a positive value on the top surface and an equal negative one at the bottom surface.

In order to account for the weld penetration present in the LCX specimens, figures of the specimens that had fatigue failure from the weld root were consulted. The width of the gap between the penetrations was measured from 9 evenly distributed spots as presented in figure 37, and these values were used to calculate the average gap width for every root sided failure. As some of the LCX specimens failed from the weld toe, thus making this method impossible/unnecessary, the root sided values were used to determine an average which would then be used for all the weld toe failures. These results are presented in table 5. As the penetration in LG specimens has no significant effect on the calculated stress concentrations and hot spot values, and the penetration is hard to determine without completely breaking the specimens, weld penetration was excluded from the LG models.

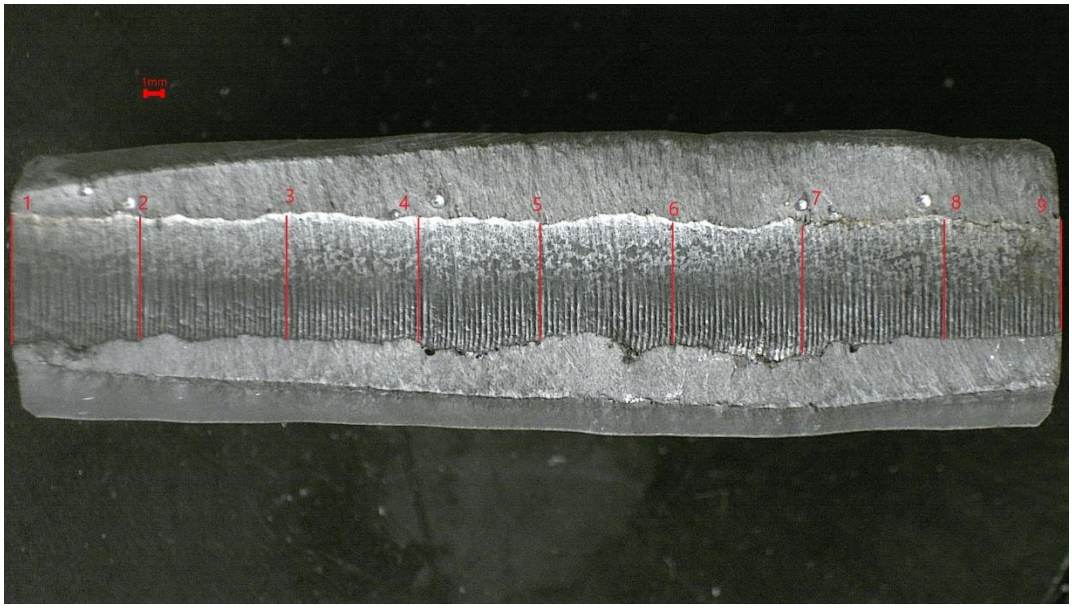

Figure 37. Measuring spots for the specimen B3 penetration gap width.

Table 5. Measured and calculated penetration gap width values.

	1	2	3	4	5	6	7	8	9	Average
B_1	5.5	5.5	5.5	6	6	6.5	6.5	7	7	6.17
B_2	3.5	3	3.5	4	4.5	4	3.5	3.5	4	3.72
B_3	6	6	6	6	5.5	5.5	6	5.5	5	5.72
C_1	2	2	2.5	2.5	2.5	3	2.5	2	2.5	2.39
C_3	3.5	4	4	4.5	4	4	3.5	3	3	3.72
									Average	4.34

4.2 Point cloud transfer methods

As previously stated, the models were constructed based on point clouds that were transferred into Femap. However, because the scans of the various specimens were performed with different methods (due to unfortunately timed maintenance of the scanning equipment), different point clouds underwent different transition methods.

The BW welds of series A were scanned with a laser into a text-file, forming a single point cloud that showcased the outline in an XY-coordinate system. As both sides were scanned separately and there did not seem to be a clear way to export text-file straight into Femap, these point clouds were first imported into SolidWorks. There the two separate point clouds representing the two sides of the specimen were aligned and spaced so that they would represent the actual specimen as closely as possible. During this the weld toes were also measured by fitting a circle into them and writing down the radius of the previously

mentioned circle. The file was saved as a DXF-file, which was then successfully imported into Femap.

The LG joints of series B (specimens B5-B8), C (specimens C5-C8) and D (specimens D1-D8) were originally scanned with a handheld Hexagon laser scanner. As previously stated, majority of the welds were scanned with 0.5 mm precision, while a couple were accidentally scanned with the precision of 1 mm. With Hexagon it was possible to set cross sections by the user, so the point clouds were formed by placing a cross section so that it would cut through the farthest-reaching point of the weld toe. These cross sections could also be used to determine the weld toe radius by fitting a circle at the weld toe, like with the BW welds, except this time the direct scanning data could be used instead of imported SolidWorks-model. The cross section point clouds could be imported as igs-files, which could then be opened in Femap without any other steps.

Finally, the LCX joints of series B (specimens 1-4) and C (specimens 1-4) were scanned with Winteria laser scanner. The program gives several point clouds in XY-coordinate system, measuring one section after another until the whole weld is covered. Out of these clouds the one in the middle of the specimen was chosen to be imported to give the overall shape of the weld. As the program gave its results in an Excel format which could not be directly imported, the middle point cloud was again imported into SolidWorks, aligned and fitted with other clouds of the same specimen and imported into Femap as a DXF-file. As for the weld toe radiuses, Winteria measured them automatically. However, the radiuses varied wildly between the sections of the same weld, so it was decided to take average of all the measured ones at the middle at a couple mm length. In the end this turned out to be unnecessary, as these radius measurements are ultimately only needed for the 4R method, which is not usable with the LCX joints due to these joints commonly breaking from the welds themselves instead of the weld toes, which isn't something that the 4R method is suited for.

4.3 Numerical analysis methods

The FE analyses were executed with the Femap's build-in analysis solver NxNastran, with Linear analysis and all the settings set to default. As the nominal stress approach only requires values that are known from the start (dimensions, loads, FAT based on weld type)

without any unknown factors or locational stress values, there was no need to create an additional set of Femap-models for nominal stress approach.

During the Femap-analysis for the hot spot values, ENS-models were used instead of new models with the original, measured weld toe radiuses. This was done in order to reduce the amount of time spent creating and running Femap-models, as it was discovered that the 1 mm weld toe radiuses for the welds did not affect the measured hot spot stress values, which is in line with previous observations by other researchers (Punkkinen 2019, p. 7). This was also valid for the root sided weld radiuses for the LG- and LCX-welds. The stress values were taken from the model by processing the maximum values of the Solid Max Principal Stress –output and then defining the values from the 0.4*t* and 1.0*t* nodes on the model.

For both the ENS- and 4R-methods Femap-models were needed to acquire the SCFs needed in the calculations. To accomplish this, these methods used models with corresponding weld toe radiuses (1 mm for ENS and r_{true} + 1 mm for 4R) which were analyzed using 1 MPa membrane and bending stress unit loads separately. After this, the SCFs of the weld toes for membrane and bending stresses were collected by reading the maximum value of the Solid Max Principal Stress –output from the model (as a 1 MPa load was used, the amount of stress at the weld toe could be converted into a SCF directly). In order to acquire some of the values needed for the 4R-analysis, a MathCAD-file presented in appendix III was used in order to calculate the unknown values σ_{max} and σ_{min} needed in the 4R analysis.

Due to the angular distortions caused by the welding process, a small bending stress will be present in each welded structure as they are attached to the testing rig and a tensile membrane stress is applied to them. As the misalignments are small and sometimes hard to accurately measure due to differing scanning methods that were used, the evaluation of the bending stress prior to testing is tedious. Because of this, an alternative method is utilized. This method uses both the measurements from the strain gauges, as well as the constructed Femap models.

During the fatigue testing, the strain gauges measured the strain at locations determined in table 4 in chapter 3.3. The strain maximum and minimum values were continuously recorded as micro strain values, spaced out by a preset amount of cycles. These values were used to

calculate the strain range at each measuring moment, which were then multiplied by 10^{-6} in order to be usable in the following calculations:

$$\Delta\varepsilon_{meas} = \left(\varepsilon_{max,meas} - \varepsilon_{min,meas}\right) \times 10^{-6} \quad (30)$$

In equation 30 $\varepsilon_{max,meas}$ is the measured maximum elongation and $\varepsilon_{min,meas}$ is the minimum value, presented in micro strain. Out of these calculated ranges, an average value at a rather low number cycle count was picked (i.e. an average value before the strain drops due to crack propagation) and recorded. After this, the strain values were measured from the FE models at the same locations were the strain gauges were attached in the real specimen. The model was subjected to a membrane stress of 1 MPa, and the nodal values were obtained by max converting the corresponding axis strain values. In other words, if the 1 MPa membrane stress was along the Y-axis, then the Y-axis strain values were max converted in order to read the nodal values. These values were also recorded and then multiplied by the stress range which was applied to the specimen during the fatigue life testing:

$$\Delta\sigma_{m,calc} = \varepsilon_{1MPa} \times \Delta\sigma_m \quad (31)$$

In equation 31 ε_{1MPa} is the strain caused by the 1 MPa stress, while $\Delta\sigma_m$ is the membrane stress range that is applied during the fatigue testing. At this point, we have both the measured strain ranges which include both the membrane and bending stress (by applying $\Delta\varepsilon_{meas}$ to equation 31), as well as the calculated strain ranges that only include the membrane stress for each strain gauge placement. With these, the bending stress range could be determined via a simple subtraction. However, it was noted that if multiple strain gauges were used in the specimen, this resulted in multiple differing values for each measuring point after the subtraction. Because of this, an average of these values was then calculated to obtain the final bending stress range:

$$\Delta\sigma_{b,i} = \Delta\sigma_{meas,i} - \Delta\sigma_{m,calc,i} \quad (32)$$

$$\Delta\sigma_b = \frac{\sum_{i=1}^{n} \Delta\sigma_{b,i}}{n} \quad (33)$$

In equation 32 $\Delta\sigma_{meas,i}$ is the measured (via fatigue test specimen) stress range with both the bending and membrane stress at a certain strain gauge position, while $\Delta\sigma_{m,calc,i}$ is the calculated (via Femap) membrane stress range at a corresponding position. $\Delta\sigma_{b,i}$ is the resulting bending stress range at the location, and in equation 33 n is the amount of strain gauges/measuring locations in the corresponding specimen. With the bending stress range determined, it was then compared to the applied membrane stress range in order to determine a bending multiplier:

$$k_b = \frac{\Delta\sigma_b}{\Delta\sigma_m} \tag{34}$$

In equation 34 $\Delta\sigma_b$ is the bending stress range of the specimen as determined previously, while $\Delta\sigma_m$ is the membrane stress range that is applied to the specimen during the fatigue life testing. The resulting multiplier can now be used to calculate the bending stresses for the Femap models: for example if the multiplier would be 0.1 for a specimen under a 100 MPa membrane stress, an additional 10 MPa bending stress would be added to the model along the original 100 MPa. All the multipliers obtained via this method are listed in table 6, which also lists the already covered bending multipliers presented in chapter 2.3.1 (both for the nominal method and the rest), as well as if the calculated average value exceeded the covered value. If the value was exceeded (because of the way the data was originally obtained, only the decimals are compared), the bending multiplier must be included in the calculations. If the bending multiplier is a negative value, its absolute value was used in the calculations. In addition, table 6 also includes the residual stresses that were measured. Only some of the specimens were measured, and as such it was decided to use the highest value for each set of specimens (A1-5, B1-4, B5-8 etc.). If a set did not have any measurements, as was the case in the LCX-welds, the default 4R value (that is equal to the base material's yield strength) was used instead.

Table 6. Calculated original and average bending stress multipliers for each specimen.

	Joint type	k_b	σ_{res}	Nom. covered	Nom. bending	Others covered	Others bending
HRO_A_1	BW	0.30	175	1.15	X	1.05	X
HRO_A_2	BW	0.34	175	1.15	X	1.05	X
HRO_A_3	BW	0.05	175	1.15		1.05	X
HRO_A_4	BW	0.19	175	1.15	X	1.05	X
HRO_A_5	BW	-0.05	175	1.15		1.05	X
HRO_B_1	LCX	0.58	235	1.45	X	1.05	X
HRO_B_2	LCX	0.02	235	1.45		1.05	
HRO_B_3	LCX	0.24	235	1.45		1.05	X
HRO_B_4	LCX	0.28	235	1.45		1.05	X
HRO_B_5	LG	0.28	573	1.25	X	1.05	X
HRO_B_6	LG	0.26	573	1.25	X	1.05	X
HRO_B_7	LG	0.15	573	1.25		1.05	X
HRO_B_8	LG	0.24	573	1.25		1.05	X
HRO_C_1	LCX	0.13	355	1.45		1.05	X
HRO_C_2	LCX	0.14	355	1.45		1.05	X
HRO_C_3	LCX	0.14	355	1.45		1.05	X
HRO_C_4	LCX	0.13	355	1.45		1.05	X
HRO_C_5	LG	0.29	605	1.25	X	1.05	X
HRO_C_6	LG	0.27	605	1.25	X	1.05	X
HRO_C_7	LG	0.27	605	1.25	X	1.05	X
HRO_C_8	LG	0.20	605	1.25		1.05	X
HRO_D_1	LG	0.15	339	1.25		1.05	X
HRO_D_2	LG	0.21	339	1.25		1.05	X
HRO_D_3	LG	0.13	339	1.25		1.05	X
HRO_D_4	LG	0.15	339	1.25		1.05	X
HRO_D_5	LG	0.09	393	1.25		1.05	X
HRO_D_6	LG	0.12	393	1.25		1.05	X
HRO_D_7	LG	0.16	393	1.25		1.05	X
HRO_D_8	LG	0.16	393	1.25		1.05	X

Because these values were obtained via strain gauge calculations and the original equation 4 for the $k_{m,eff}$ in chapter 2.3.1 used values obtained via idealized misalignment formulae, it was decided to use the k_b values from table 6 as the bending stress multipliers, instead of putting them through further equations.

5 RESULTS

Obtained results included the fatigue life test results, fatigue strength assessment results and the quality of the welds, all of which are presented below in their own chapters.

5.1 Fatigue test results

The results of the fatigue tests are presented below in table 7. The plate width and thickness, b_{ideal} and t_{ideal} respectively, are presented in the said table as idealized values, with the actual values differing slightly (for example, 7.93 mm thickness would be presented as 8 mm). The highest difference between the actual measurement and the idealized one was 0.9 mm in the case of width and 0.6 mm in the case of thickness. In the case of thickness this maximum value was an outliner, with the average difference being between 0.02-0.05 mm. The exceptions to this are those LCX-welds that broke from the root side, as for these welds the plate thickness was replaced with the combined effective throat thickness. These values can easily be identified by the included decimals.

Table 7. Fatigue test results.

	F_{max} [kN]	F_{min} [kN]	R	Joint type	b_{ideal} [mm]	t_{ideal} [mm]	N_f
HRO_A_1	240	24	0.1	BW	60	8	84026
HRO_A_2	220	22	0.1	BW	60	8	130792
HRO_A_3	200	20	0.1	BW	60	8	415137
HRO_A_4	240	24	0.1	BW	60	8	171073
HRO_A_5	220	22	0.1	BW	60	8	83959
HRO_B_1	110	11	0.1	LCX	60	11.56	188216
HRO_B_2	90	9	0.1	LCX	60	12.75	562833
HRO_B_3	130	13	0.1	LCX	60	12.59	136012
HRO_B_4	140	14	0.1	LCX	60	10	110496
HRO_B_5	130	13	0.1	LG	80	8	244599
HRO_B_6	240	120	0.5	LG	80	8	158076
HRO_B_7	110	11	0.1	LG	80	8	307107
HRO_B_8	200	100	0.5	LG	80	8	506290
HRO_C_1	170	17	0.1	LCX	60	14.06	224446
HRO_C_2	130	13	0.1	LCX	60	12	1469011
HRO_C_3	150	15	0.1	LCX	60	12.58	188028
HRO_C_4	160	16	0.1	LCX	60	12	286336

Table 7 continues. Fatigue test results.

	F_{max} [kN]	F_{min} [kN]	R	Joint type	b_{ideal} [mm]	t_{ideal} [mm]	N_f
HRO_C_5	130	13	0.1	LG	80	8	164304
HRO_C_6	110	11	0.1	LG	80	8	274115
HRO_C_7	200	100	0.5	LG	80	8	227987
HRO_C_8	240	120	0.5	LG	80	8	174614
HRO_D_1	130	13	0.1	LG	80	8	701033
HRO_D_2	240	120	0.5	LG	80	8	638517
HRO_D_3	150	15	0.1	LG	80	8	346631
HRO_D_4	270	135	0.5	LG	80	8	290460
HRO_D_5	130	13	0.1	LG	80	8	430809
HRO_D_6	150	15	0.1	LG	80	8	216501
HRO_D_7	270	135	0.5	LG	80	8	128975
HRO_D_8	240	120	0.5	LG	80	8	277350

As previously mentioned, the S-N curves were formed via the so-called "Standard procedure" (Hobbacher 2016). The calculations for 97.7 % and 50 % survival probability curves were performed in Excel according to the equations presented in chapter 2.4 and plotted in the same figure, along with the stress range and fatigue life values for each welded specimen. Various values used in these calculations are listed in the appendix IV for verification, including the FAT values for 50 % and 97.7 % curves at the $2x10^6$ cycles. For the first round these calculations used the calculated *m* value even if the number of specimens was below 10. After this the calculations were performed again, but this time with the fixed *m* value of 3. This was done so that the mathematically correct curves could be obtained (fixed for butt and LG welds, calculated for LCX), as well as the "wrong" ones in order to compare the difference caused by these calculations. Finally, curves based on the basis shear stresses were calculated using the *m* value of 5. These curves were the most unimportant but were included just in case. Figure 38 contains the S-N curves with free, fixed and shear-based slopes for BW welds, figure 39 for LCX welds and finally figure 40 for LG welds. These graphs also contain the approximate standard S-N curve for the FAT class of each weld joint type. The red dots exemplify a stress ratio R of 0.1, while the black dots exemplify either root sided failure (figure 39) or a stress ratio of 0.5 (figure 40).

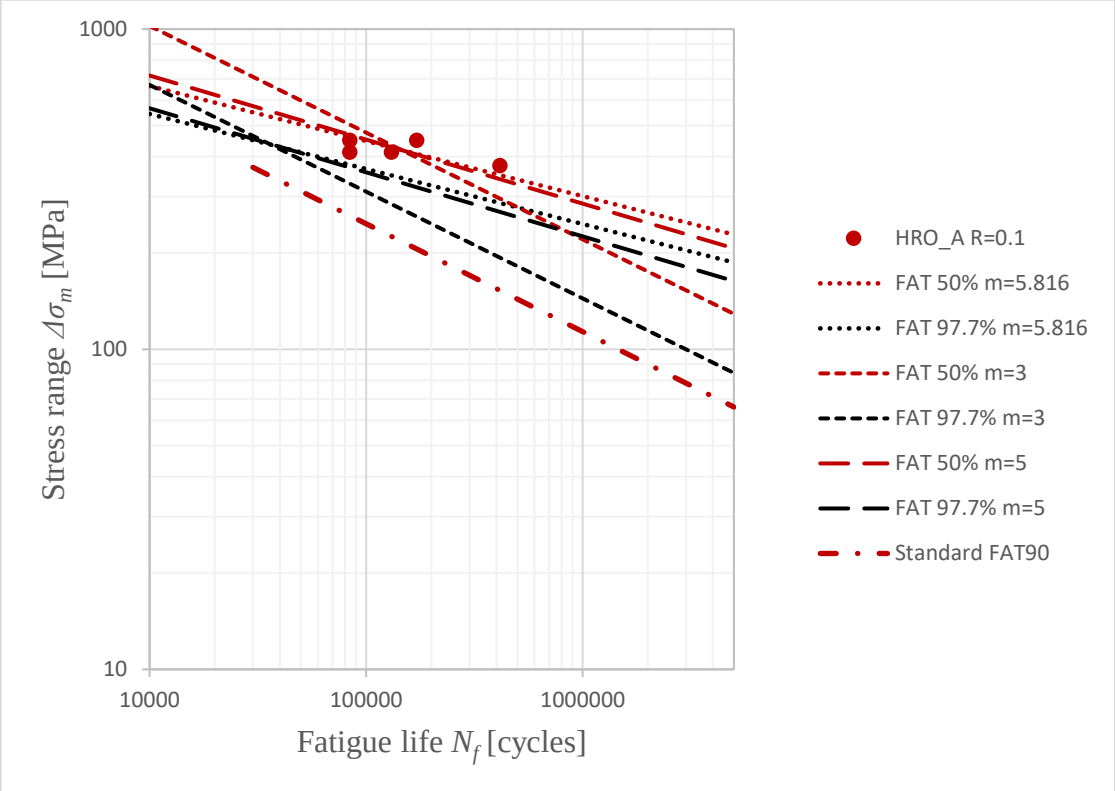

Figure 38. S-N curves of the BW welds with free, fixed and shear-based *m* values, and the standard S-N curve for FAT 90.

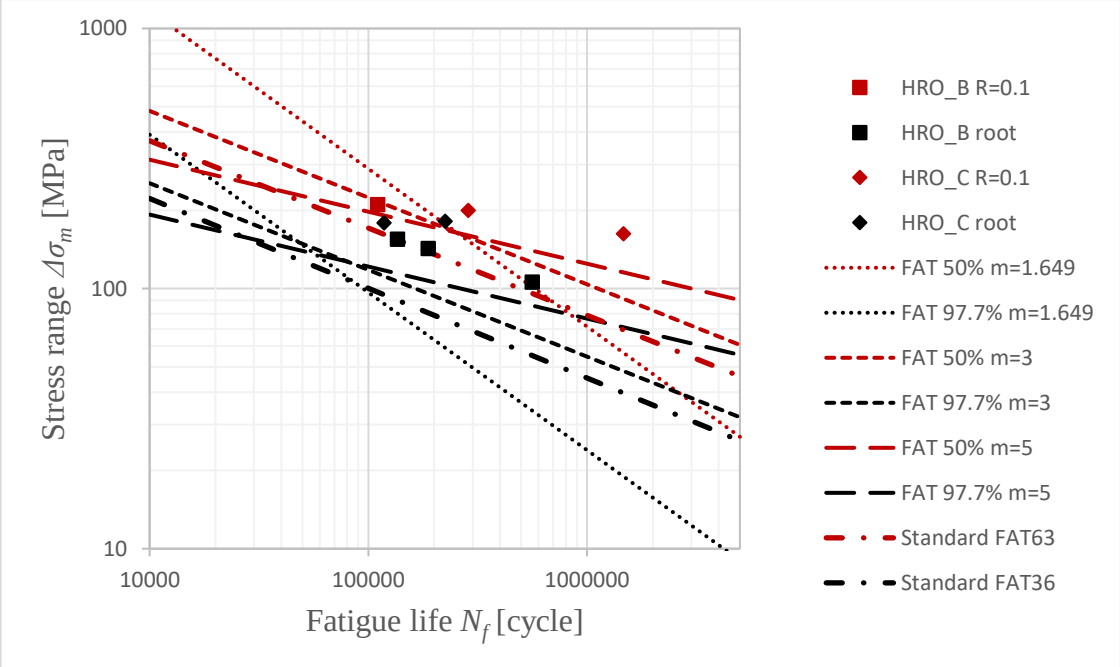

Figure 39. S-N curves of the LCX welds with free, fixed and shear-based *m* values, and the standard S-N curves for FAT 63 and 36.

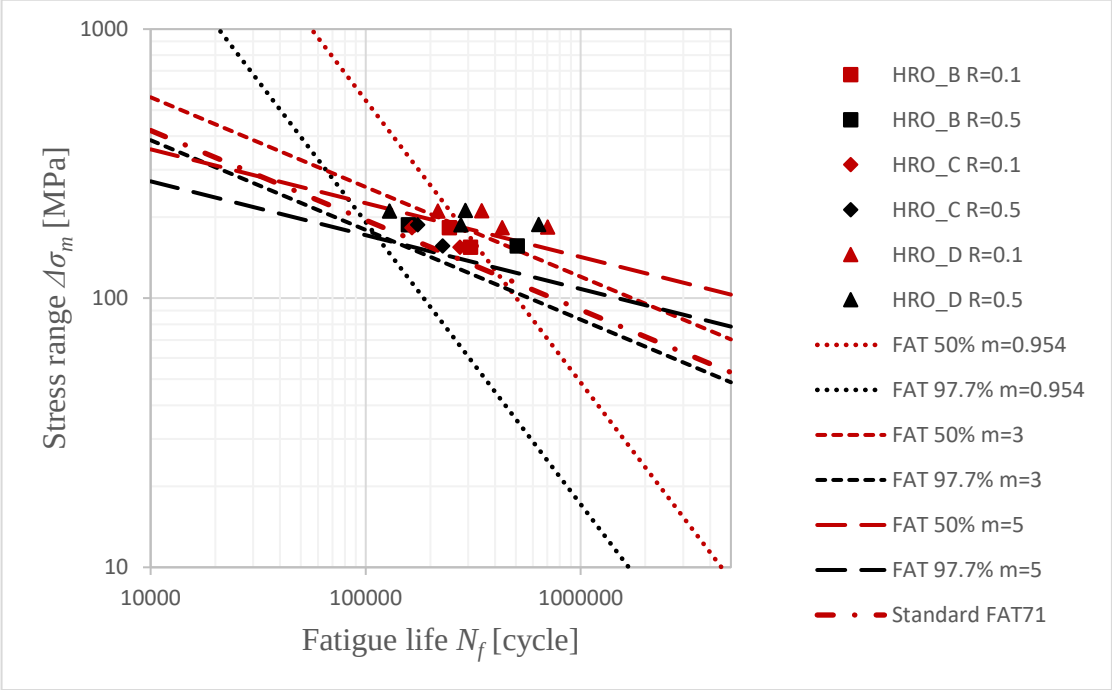

Figure 40. S-N curves of the LG welds with free, fixed and shear-based *m* values, and the standard S-N curve for FAT 71.

5.2 Numerical analysis results

Fatigue life estimations provided by the various numerical methods have been listed in the table 8, alongside with fatigue test results to illustrate the difference between the computational and experimental fatigue lives. If the specimen was made using multiple materials, the weaker material's values were used in calculations, as all the series A welds broke from the root side. In addition, if an LCX specimen broke from the root side, it was excluded from both the hot spot and 4R calculations, as these methods do not have enough reference material to validate and confirm the results. Table 9 presents the total accuracy of the various numerical methods: first by listing how many of the calculated cycle values were "safe" (calculated value below the test result, in other words the specimen lasted longer than expected by the calculations) and then by presenting the percentage value of the same statistics. Appendix V showcases the relation between the test results and calculated values, as well as the average values for each calculation method. These values show how many times calculated value can be included in the test value: values above 1 mean that the specimen lasted longer than projected in the calculations, while values below 1 mean that the specimen broke before the calculated cycle value could be reached. These results are also exemplified in the graphs of figures 41 and 42. The calculated fatigue strength assessment

approach results are on the horizontal x-axis while the experimental testing results are on the vertical y-axis. The results are presented with markers, categorized by the series A-D and the value of stress ratio *R* of 0.1 (red) or 0.5 (black). If the dot is above the grey corner-to-corner middle line, it means that the specimen in question lasted longer in fatigue testing than the calculated fatigue life indicated. Finally, figure 43 compares the results between the normal 50 % probability 4R calculation and the one utilizing the alternative values which were found later (Ahola et al. 2019b).

Table 8. Fatigue life expectancy according to numerical methods.

	Nom. 97.7 %	Nom. 50 %	Hot spot 97.7 %	Hot spot 50 %	ENS 97.7 %	ENS 50 %	4R 97.7 %	4R 50 %	Ahola 4R 50 %	Test results
A_1	6934	17829	7192	18492	27681	71178	12628	72666	93940	84026
A_2	8179	21030	12977	33368	75541	194243	33982	195546	206339	130792
A_3	26062	67014	23718	60988	74346	191171	44277	254788	254646	415132
A_4	9040	23244	9274	23847	38278	98425	17662	101634	122652	171073
A_5	19212	49400	17631	45336	57822	148682	40265	231698	236126	83959
B_1	8136	20919	-	-	49649	127664	-	-	-	188216
B_2	78608	202129	-	-	504126	1296285	-	-	-	562833
B_3	25114	64576	-	-	75080	193058	-	-	-	136012
B_4	10076	138853	36842	94734	62241	160044	168552	969915	736892	110496
B_5	56709	145820	24026	61778	169400	435588	68178	392323	358879	244599
B_6	54282	139579	24521	63052	141689	364331	53018	305088	293855	158076
B_7	193391	497278	62769	161401	213548	549107	126001	725061	584742	307107
B_8	189052	486120	44719	114988	224238	576594	105946	609654	509469	506290
C_1	15641	40219	-	-	221956	570726	-	-	-	224446
C_2	116544	299677	99495	255837	385182	990438	924029	5317231	2849546	1469011
C_3	16309	41937	-	-	129291	332452	-	-	-	188028
C_4	62512	160740	57915	148921	214784	552287	421639	2426276	1527309	286336
C_5	53765	138248	24429	62814	154971	398486	78587	452218	401786	164304
C_6	94942	244130	41035	105516	252309	648775	138644	797812	630917	274115
C_7	90916	233778	38914	100060	160653	413096	77963	448631	399250	227987
C_8	109409	281330	27699	71223	123159	316686	49996	287699	280462	174614
D_1	115416	296774	34141	87789	140355	360903	113164	651190	536871	701033
D_2	107779	277138	26254	67508	120121	308873	60025	345408	324326	638517
D_3	75698	194645	22512	57888	95785	246297	88578	509716	441888	346631
D_4	74849	192462	22222	57141	107007	275152	53712	309079	296906	290460
D_5	118043	303530	38805	99782	185387	476694	171531	987060	747227	430809
D_6	76554	196847	22914	58919	110023	282909	71319	410397	371959	216501
D_7	75698	194645	19354	49765	72107	185412	38973	224264	230084	128975
D_8	107781	277143	30395	78156	134483	345802	53858	309920	297548	277350

Table 9. Total accuracy of the numerical methods (amount of calculated values higher than the test results).

	Nom. 97.7 %	Nom. 50 %	Hot spot 97.7 %	Hot spot 50 %	ENS 97.7 %	ENS 50 %	4R 97.7 %	4R 50 %	Ahola 4R 50 %
#	29/29	24/29	24/24	24/24	29/29	9/29	22/24	5/24	4/24
%	100 %	82.76 %	100 %	100 %	100 %	31.03 %	91.67 %	23.81 %	16.67 %

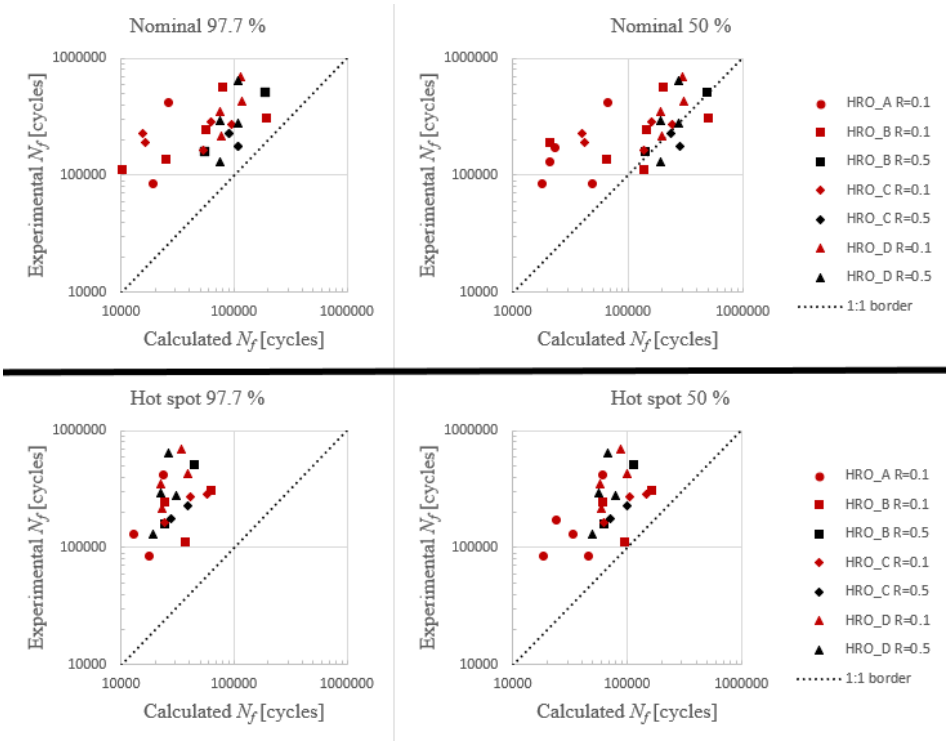

Figure 41. Comparison of calculated (x-axis) and experimental (y-axis) fatigue life of nominal and hot spot methods.

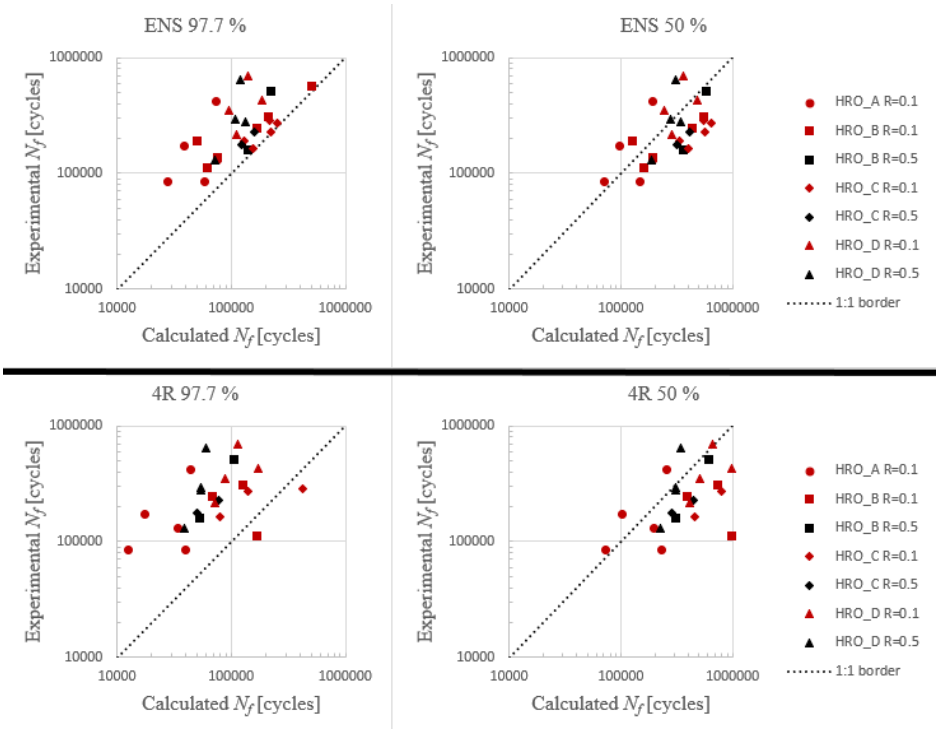

Figure 42. Comparison of calculated (x-axis) and experimental (y-axis) fatigue life of ENS and 4R methods.

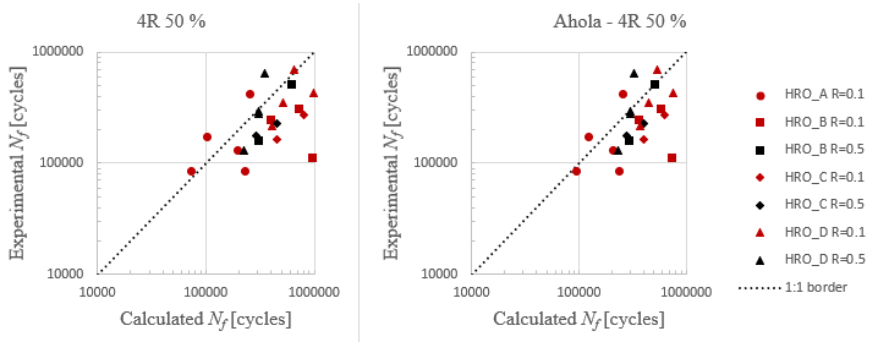

Figure 43. Comparison of calculated (x-axis) and experimental (y-axis) fatigue life of normal 50% 4R method and 50% method utilizing the values of D. Sc. Ahola.

5.3 Quality according to EN ISO 5817

The results for the weld joint quality are listed in table 10. For the meaning of each imperfection number, refer to table 2 in chapter 2.5. The insufficient/excessive throat thickness values (1.20 and 1.21) for LCX-welds are in brackets as according to the standard these measurements are not applicable if there is proof of greater weld penetration, and thanks to the pictures of the broken LCX-welds, there is. In addition, if the insufficient throat thickness (1.20) is ranked below B, the excessive thickness (1.21) value is replaced with a

dash (-), as the thickness is clearly below ideal value and thus cannot achieve an excessive value. Visual breakdown of these identification numbers is presented in figure 44.

Table 10. Quality of the welded joints according to ISO 5817.

		1.6	1.7	1.9	1.10	1.11	1.12	1.14	1.16	1.17	1.20	1.21	3.1
A1	BW	B	B	B		B	B	B		B			B
A2	BW	B	B	B		B	B	B		B			B
A3	BW	B	B	B		B	B	B		B			B
A4	BW	B	B	B		B	B	B		B			B
A5	BW	B	B	B		B	B	B		B			B
B1	LCX		B		B		B		B		(B)	(B)	
B2	LCX		B		B		B		B		(C)	-	
B3	LCX		B		B		B		B		(B)	(B)	
B4	LCX		B		B		B		C		(B)	(B)	
B5	LG		C		B		B		D		B	B	
B6	LG		D		B		B		D		B	B	
B7	LG		B		B		B		D		C	-	
B8	LG		B		B		B		D		C	-	
C1	LCX		B		B		B		C		(D)	-	
C2	LCX		B		B		B		D		(D)	-	
C3	LCX		B		B		B		D		(D)	-	
C4	LCX		B		B		B		D		(D)	-	
C5	LG		B		B		B		D		B	B	
C6	LG		B		B		B		D		B	B	
C7	LG		B		B		B		D		C	-	
C8	LG		D		B		B		D		B	B	
D1	LG		B		B		B		D		D	-	
D2	LG		D		B		B		D		C	-	
D3	LG		B		B		B		D		C	-	
D4	LG		B		B		B		D		D	-	

Table 10 continues. Quality of the welded joints according to ISO 5817.

		1.6	1.7	1.9	1.10	1.11	1.12	1.14	1.16	1.17	1.20	1.21	3.1
D5	LG		B		B		B		D		C	-	
D6	LG		B		B		B		D		C	-	
D7	LG		B		B		B		B		C	-	
D8	LG		D		B		B		D		C	-	

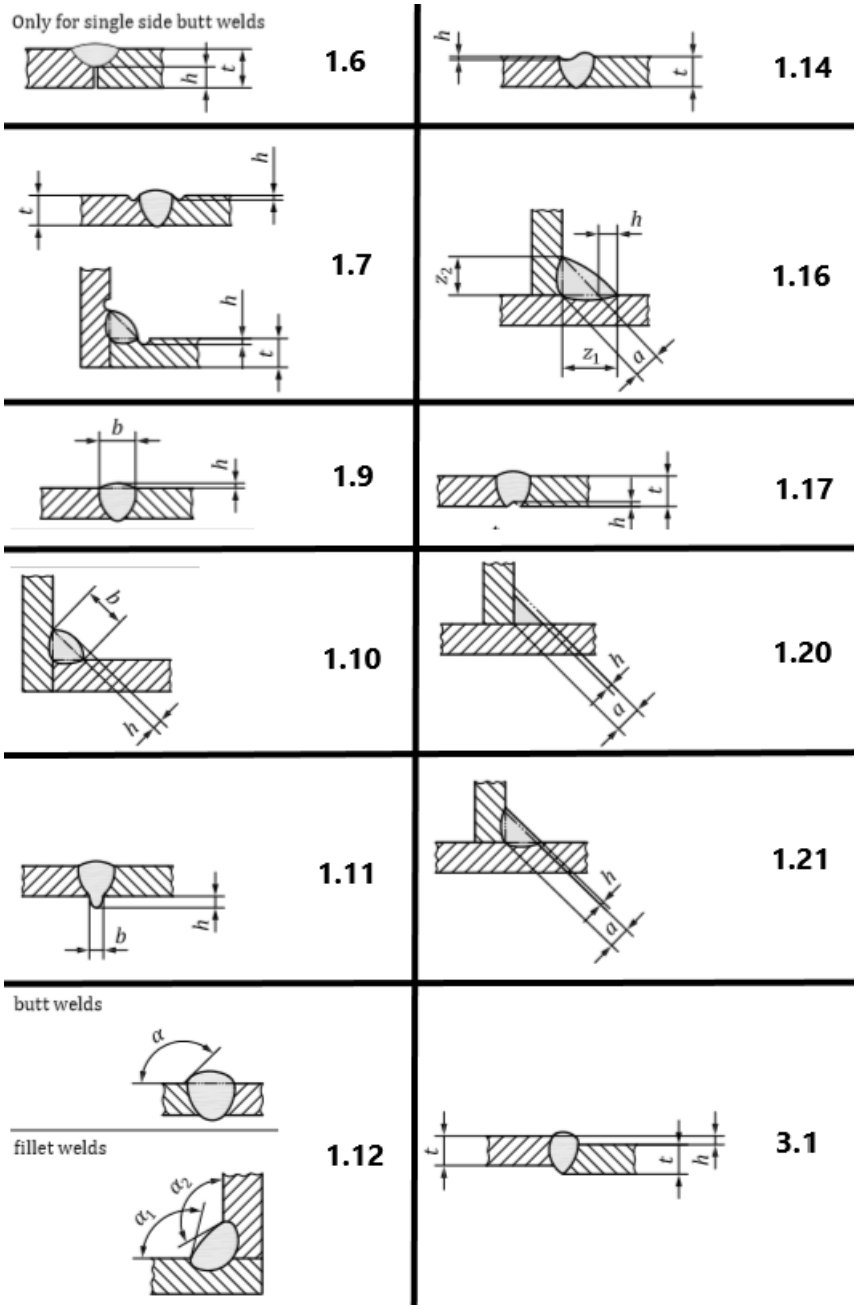

Figure 44. Visual breakdown of the weld quality identification numbers (ISO 5817 2014, p. 17-30).

6 DISCUSSION

In the following chapters the general observations, suitability, limitations/issues and influencing factors of the test and calculation results are discussed.

6.1 General observations

Based on the results compiled previously in tables 7 and 8 of chapter 5.2, the survival probabilities for different calculation methods were partly as expected and partly not: when calculating the 97.7 % probabilities, both the nominal and hot spot methods had 100 % rate of "successful results", in this case meaning that the results were below the tested fatigue results, further meaning that all the specimens survived longer than expected when compared to the calculations. Concerning ENS and 4R methods, the amount of successful results was basically the wanted 97.7 %, as they both had only one inaccurate prediction.

However, concerning 50 % probabilities nominal stress and hot spot both had an over 50 % rate for the successful results, with practically 80 % of the nominal results and every single of the hot spot results being successful. ENS and 4R had a weaker amount of successful results at 31 % and below, and in the case of 4R, Ahola's 4R method had one less successful result when compared to the default 4R method. It should be noted that 4R is missing 8 results that the other methods apart from hot spot have access to, reducing the amount of comparable results roughly by a quarter.

In figures 45, 46 and 47 the results are plotted similarly as in the numerical analysis of chapter 5.2, but this time they are separated based on the joint type and they showcase how premature fatigue failure (dot below the 1:1 border) is related to the corresponding joint type. According to these figures, both the BW and LCX results tended to be on a safer side than the LG results in nominal method. In hot spot and ENS methods all the results seem to spread at roughly the same general distance from the border, although the low amount of LCX results in hot spot (due to root sided failures being excluded) means one cannot be sure about them. In 4R the BW and LG results inhabit the same general space, and the LCX results noticeably further away, and make up the entirety of the failed 97.7 % predictions. Based on these results the ENS seems to be the best method for multiple different joints, as all the

results are clumped together, regardless of the joint type, and its FAT 50 % success rate is the closest one to a 50/50 split (31 %).

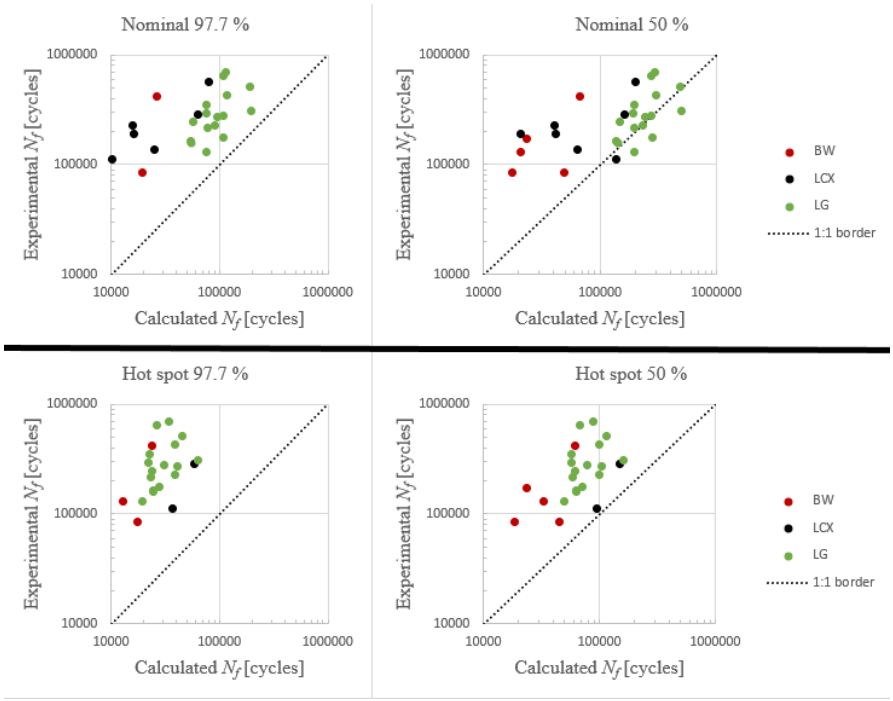

Figure 45. Comparison of calculated (x-axis) and experimental (y-axis) fatigue life of nominal and hot spot methods by joint type.

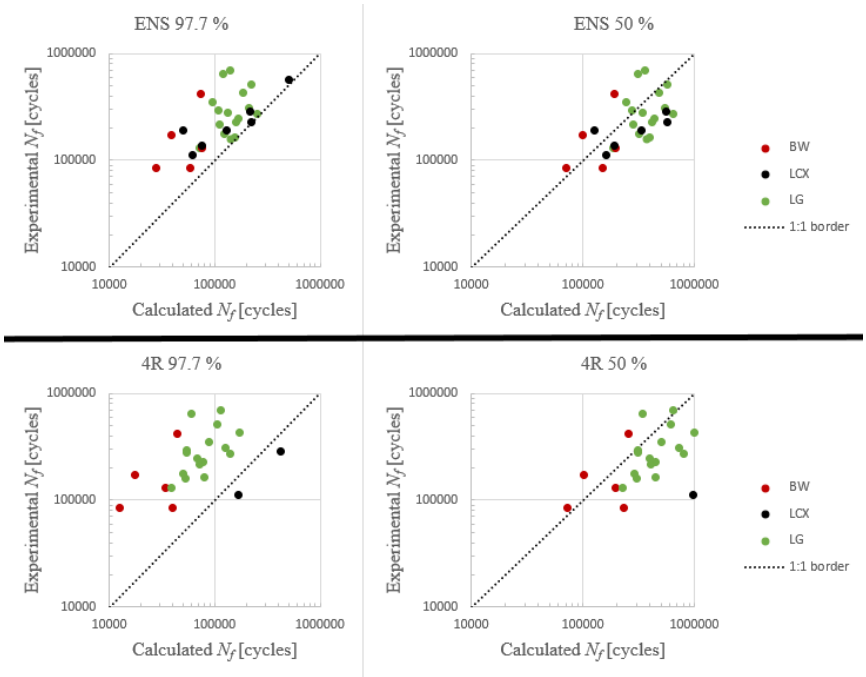

Figure 46. Comparison of calculated (x-axis) and experimental (y-axis) fatigue life of ENS and 4R methods by joint type.

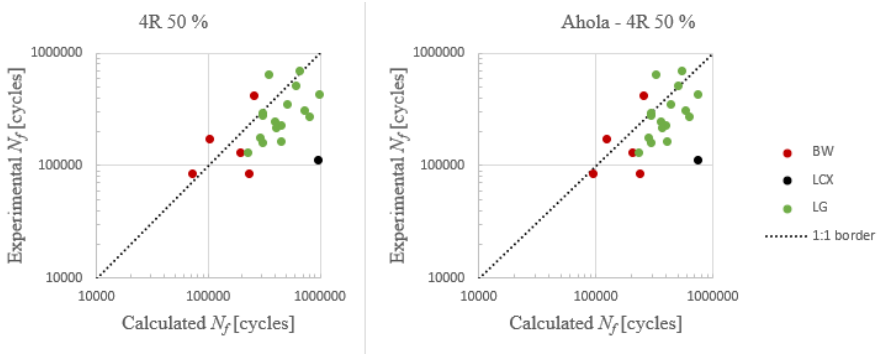

Figure 47. Comparison of calculated (x-axis) and experimental (y-axis) fatigue life of normal 50% 4R method and 50% method utilizing the values of D. Sc. Ahola by joint type.

According to the S-N curves all specimens exceeded the 97.7 % survival probability, regardless if they used the free or fixed curve. The 50 % probability was less consistent as shown in table 11, which showcases both the numerical and percent number of specimens that cleared this curve. There were only three cases where 50 % of the results would exceed their calculated fatigue life expectations, while in most cases the amount of exceeding results was roughly around 40 %. The free, fixed and shear-based butt weld curves resulted in the same number of specimens clearing the 50 % line, while the LCX and LG welds had small difference between the three values. In the LCX case the free and shear-based curves resulted in a 50/50 split of the results while roughly 40 % of the results crossed the fixed curve, which is surprising as this set has below 10 specimens in it, making it so that the fixed value should be reliable and more accurate, at least on paper. The LG case mirrored this with the 50/50 split happening at the fixed curve, which is again surprising as this set had above 10 specimens in it, which should mean that the free curve should be accurate enough and the results wouldn't be so scattered.

Table 11. Numerical and percent amounts of specimens that cleared the 97.7 % and 50 % S-N curves, free, fixed and shear-based.

	Free 97.7 %	Free 50 %	Fixed 97.7 %	Fixed 50 %	Shear 97.7 %	Shear 50 %
Butt	5/5	2/5	5/5	2/5	5/5	2/5
LCX	8/8	4/8	8/8	3/8	16/16	4/8
LG	16/16	6/16	16/16	8/16	8/8	7/16

Table 11 continues. Numerical and percent amounts of specimens that cleared the 97.7 % and 50 % S-N curves, free, fixed and shear-based.

	Free 97.7 %	Free 50 %	Fixed 97.7 %	Fixed 50 %	Shear 97.7 %	Shear 50 %
Butt [%]	100.0 %	40.0 %	100.0 %	40.0 %	100.0 %	40.0 %
LCX [%]	100.0 %	50.0 %	100.0 %	37.5 %	100.0 %	50.0 %
LG [%]	100.0 %	37.5 %	100.0 %	50.0 %	100.0 %	43.8 %

It should be noted that the calculated *m* values for the LCX and LG welds in S-N curves (figures 39 and 40) were surprisingly low, as a fixed curve uses *m* value of 3 and the calculated values were noticeably below 2, but at the time these were thought to be the result of low amount of specimens. After the S-N results were calculated and listed, it was noted that the BW welds (figure 38) had relatively normal calculated *m* values, despite a similarly low number of specimens. After a short amount testing showcased in table 12, it was noted that mixing specimens from different companies together seemed to distort the calculation results. When the LCX values are calculated for companies 2 and 3 separately, there is a clear difference in the results. Similarly, when the LG values are separate, each of the companies 2, 3 and 4 get different results. Additionally, company 4 had the specimens 1-4 and 5-8 made from different materials, but the calculated *m* values are roughly the same regardless if these two sets of specimens were used together or not. This seems to indicate that the different methods used by different companies affect the *m* values in a way that creates the need for individual calculations for each of them, but the amount of specimens is far too low in order to make any decisive conclusions.

Table 12. Comparison of calculated m values when companies are together and separated.

		Original m		Separated m
LCX	B1-4 C1-4	1,649	B1-4	2,394
			C1-4	7,572
LG	B5-8 C5-8 D1-4 D5-8	0,954	B5-8	4,033
			C5-8	2,207
			D1-4	5,685
			D5-8	5,791
			D1-4 D5-8	5,58

6.2 Suitability of the methods

With the nominal stress method, 100 % of the results exceeded the 97.7 % survival predictions and 82.76 % exceeded the 50 % predictions. These results are heavily skewed on the safe side and contain a lot of scatter as shown in the figure 41 in chapter 5.2, meaning that they do not give reliable results that could be used for reliable and precise fatigue life predictions. This highlights the need for more precise methods that take account of the effects of the weld toe.

The hot spot method is the most inaccurate method, as 100 % of the results exceeded both the 97.7 % and 50 % predictions. As can be seen from appendix V, the test results/calculations ratios of these results, as well as their average values, are much higher than all the other methods, which means that the calculated values were noticeably smaller than with other methods. This would at first indicate that the method is not suitable for fatigue life predictions, but as the method is presented in the official IIW recommendations (Hobbacher 2016, p. 18-27), it is more likely that something has gone wrong in the hot spot measuring process. However, at the time of the research there was not a clear indication what might have gone wrong, meaning that the method and its results must be sidelined for now.

The ENS method had all the results exceed the 97.7 % prediction, while 31.03 % of the results exceeded the 50 % prediction. While this is below the ideal 50/50 split and majority the markers are very close to the border line in figure 42, it is more precise and has less deviation than the nominal method when it comes to the 50 % prediction, meaning that it can be used to predict the fatigue life limit in a more reliable method that is more likely to give actual directive results.

The 4R method had all but two of the specimens exceed the 97.7 % prediction while being greatly on the safe side of the border line as seen in figure 42, and the 23.81 % of the specimens that exceeded the 50 % prediction were packed near the border even if they didn't achieve the wanted 50/50 split. When using the alternative values (Ahola et al. 2019b) for the 50 % calculations, the results are almost the same (as shown in figure 43) with a total of one less specimen crossing the border, but the results are slightly more packed together near the border.

Out of all the four methods, either ENS or 4R seems to be the best suited one, even if they did not achieve the 50/50 split on the 50 % predictions as was hoped. 4R might be better for a guaranteed fatigue life estimation because the 97.7 % results are clearly on the safe side (discounting the two that failed) unlike in ENS where multiple specimens could dip below the border with even the slightest deviation. On the other hand, for the 50 % predictions, while majority of them were below the border, the ENS results were more stacked, more successful and closer to the border than the 4R results, although the 4R results improved slightly when Ahola's values were used by moving closer to the border (while the amount of results clearing the border dropped by one). This would indicate that the ENS is less likely to suffer from random deviations and does not provide as overly optimistic results as the nominal method. Both the ENS and 4R methods take note of the weld toe and the concentrations that it causes, unlike the nominal method that uses predetermined FAT values that might not represent the actual situation. In short, 4R seems to give safer 97.7 % results most of the time, while ENS seems to give safer and more reliable 50 % results. However, as shown by Ahola's values, this could be a result of improper 4R values, which could be remedied with appropriate adjustment of said values.

6.3 Limitations and issues

Perhaps the most notable limitation is related to the bending stresses. As established previously, these were formed as a relation to the normal stresses, and these relations in turn were based on the calculations which were carried out utilizing the strain gauge measurements. The problem is that these gauge readings tended to be somewhat inconsistent, and if the specimen had two or more gauges, they would always result in different bending values, which would then be combined into an average. In addition, sometimes the gauges would be placed on both sides of the welded middle piece, sometimes only one side would have gauges and the weld would break from the opposing side, resulting in suboptimal readings. These inconsistences could possibly then lead to inconsistent bending values. And because the sample size is relatively small and full of different types of welds by different welders, there is no certainty that the bending values are completely reliable, meaning that the possible inconsistences have more impact than they would in a larger sample size. Possible fix would have been to make the use of gauges uniform: each specimen would have strain gauges at both sides of the middle-welded part (unless one side had been HFMI

hammered). In addition, the sample size should probably have been larger in order to weed out some of the inevitable measuring/gauge placement mistakes.

Another issue is the fact that the weld toe radiuses were measured from the scanning programs or point clouds. As these methods have a limited precision and the measuring was primary executed with a circle placement, it is likely that some mistakes have happened. This is especially likely with the Winteria measurements, as it measured multiple, differing results for one weld toe that were then formed into an average. As a result of these inaccuracies, it is possible that some of the modeled weld toes do not represent the actual weld toes correctly, thus influencing the Femap results, especially the SCFs. A possible solution would have been to measure the weld toe radiuses physically from the test specimens before fatigue testing, preferably with the help of an experienced person, in order to avoid the inaccuracies presented by the models, point clouds and scanner readings. Another would have been to use a uniform measuring method for all the welds, eliminating any possible mistakes that the differing methods would cause in relation to each other.

6.4 Influencing factors

According to the ISO standard, the specimens were mostly of a high B quality, especially the butt welds (A1-5) all of which scored B in every reviewed aspect. When it comes to the LCX (B1-4 and C1-4) and LG (B5-8, C5-8 and D1-8) specimens, they mostly had a decent number of Bs as well, except for the excessive asymmetry of the fillet weld and insufficient throat thickness, which were present in practically every specimen. The insufficient throat thicknesses could be ignored in the LCX welds as there was enough proof via the root-sided failures that the specimens had additional penetration in addition to the lackluster a-measurement. However, in the case LG welds there was no such way to confirm additional weld penetration, meaning that they had to be listed as subpar if they did not achieve acceptable value without the penetration. Few specimens also suffered from the intermittent undercut, but in every case, this was present at the attached part's weld toe, not the critical one of the base materials. Because the defects were so universal and specific, it is hard to say if they affected the results in the end, as there isn't a set of flawless LCX specimens and a set of flawed LCX specimens that could be compared to each other, only flawed ones. However, if the practically flawless butt welds are compared to the rest of the flawed welds via the fatigue life expectancy of the figures of chapter 5.2, the flawless butt welds scored

better than the rest, their markers being located at a longer distance from the 1:1 border at the safe side. But the number of specimens is too small to draw any conclusive deductions.

Regarding SCFs, previous studies have found out that the weld size has a major effect on them, especially the weld toe angle (Gurney 1979, p. 28-29). According to previous research, the weld toe angle increasing also increases the SCF practically linearly, at least up to 55°. In addition, the research shows that the weld size's influence on the SCF depends on the weld type: non-load-carrying or load-carrying. According to the research the SCF in non-load-carrying joints tends to increase as the weld size increases, while with load-carrying joints the SCF decreases as the weld size increases. (Gurney 1979, p. 28-29) On a quick glance there would seem to be truth to this: B1-4 and C1-4 consisted of load carrying LCX-welds, with the B series consisting of very symmetrical welds, while C series consisted of very asymmetrical welds. This would indicate that the welds of series C were larger, and coincidentally the SCFs of these welds were larger than those of the series B as shown in appendix VI. Previous research has also shown that SCF at the weld toe tends to increase with increasing ratio between the thickness of the attachments and the thickness of the main plate (Gurney 1979, p. 123). Assuming this ratio is attachment divided with main plate, this would give the series B a ratio of 1 and series C a ratio of 3.33. However, as can be seen from the appendix VI, series B has the higher SCFs out of the two, meaning that this theory does not seem to apply here. However, because the number of values is so small at eight specimens, and there are differences in the weld symmetry between the two series, which also affects the SCFs, these results cannot be used to perform any definitive conclusions without further research.

When comparing the SCFs obtained via FEA for both ENS and 4R methods, in almost every case the ENS values are higher, both in normal and bending stress. Because the models used to obtain these values were same between the two methods, apart from the weld toe radiuses (the ENS models had weld toe radiuses of 1 mm while 4R had the addition of the measured value), it shows that larger weld toes reduce the SCF, thus reducing the stress in the weld toe, which in turn improves the fatigue life. It should be noted that only the results of both BW and LCX welds were compared, as the hot spot and 4R values for LG welds were not calculated due to method not working with said weld type.

7 CONCLUSIONS

All the series cleared the 97.7 % prediction in both the S-N curves and various methods, excluding a couple of individual results. However, in the 50 % predictions there were a lot of differences. While both the nominal and hot spot gave overtly positive results (hot spot to the point that something has probably gone wrong), both the ENS and 4R underperformed. While using ENS resulted in more specimens exceeding their calculated fatigue life predictions and thus making it the more reliable method, 4R could possibly be the better method in the long run, as it was shown that the alternative 50 % values do affect the results, causing them to move closer to the 1:1 border. S-N curves performed better, as all the results cleared the 97.7 % prediction, and the values for the 50 % predictions were either 50 % or close to 40 %. However, it seems that mixing specimens from different companies together in the curve calculations can result in weird angles for said curves. In order to conduct reliable fatigue life predictions beyond the 97.7 % survival probability, it is necessary to account for the SCFs, as the overtly positive nominal and hot spot methods exemplified. In short to answer the first research question, “which methods are applicable for fatigue strength assessment of welded details at workshop quality”, both the ENS and 4R seem to be the best ones, with ENS winning due to more reliable 50 % survival probability results, and as 4R will require a further look into the used variables and values in order to achieve the wanted 50 % survival probability.

Many welds suffered from imperfections: mainly insufficient throat thickness and asymmetry of the weld. When compared to the A series that had no such imperfections, the A series performed better, although this could be a result of differing joint types. In future the weld quality should be paid additional attention to in order to determine for sure if the weld quality is a major factor compared to joint type. So, to answer the second question, “What are the factors influencing the fatigue strength capacity in the studied joints”, the weld quality seems to be a big factor, assuming that it is not cancelled out by the joint type. Beyond this the joint type was also a factor, as most of the LCX joints could not be used in half of the methods, including the 4R which the one that was the most interesting one. In addition, in 4R the LCX joints had the worst performance. Finally, when comparing the ENS and 4R

models, the weld toe radius *r* used in the modeling has a notable effect on the SCFs and thus the results.

In the future the scanning methods should be unified. Because three vastly differing scanning methods were used, there is no guarantee that the transferred FEA models have a same level of accuracy. In addition, the method for resolving the bending stresses could probably use at least a review, as different gauges in a same specimen result in different bending stresses, which would then be averaged. There were also situations in which the specimen broke from a side that did not have any gauges, meaning that in the future both sides should have gauges unless it is certain (via HFMI) that the specimen will break from one side. The S-N curves also need to be examined further to see if mixing specimens from different origins truly has negative effects on the calculated *m* values as the results seemed to indicate.

Finally, to answer the final question, "which fatigue-related factors should be determined precisely, and in which case, default or conservative assumptions can be made", obviously factors that affect the calculation process such as the bending multiplier k_b and SCFs should be determined precisely, which in turn means that weld toe radius *r* needs to be determined precisely. As for factors that are not so critical, these would include more secondary factors like the precise shape of the weld (if the throat thickness and overall shape are accounted).

LIST OF REFERENCES

Ahola, A., Björk, T. & Skriko, T. 2019a. Determination of S-N Curves [web document]. Lappeenranta: April 2019. [Referred 10.3.2020]. Licentiate's teaching material. Lappeenranta-Lahti University of Technology LUT. 19 p. Available in PDF-file: https://moodle.lut.fi/pluginfile.php/422694/mod_resource/content/2/S-N%20curves.pdf Service needs a LUT account.

Ahola, A., Skriko, T. & Björk, T. 2019b. Fatigue strength assessment of ultra-high-strength steel fillet weld joints using 4R method. In: Journal of Construction Steel research. 12 p. Available: https://www.sciencedirect.com/science/article/pii/S0143974X19310223

Ahola, A. 2020a. 4R_Method.pdf [private e-mail]. Receiver: Otto Ratala. Sent 17.1.2020, 8.43 o'clock (GMT +0200). Attachment: "4R_Method.pdf"

Ahola, A. 2020b. Jännityskertoimet ja S-N kaavat [private e-mail]. Receiver: Otto Ratala. Sent 9.3.2020, 13.11 o'clock (GMT +0200).

Björk, T., Mettänen, H., Ahola, A., Lindgren, M. & Terva, J. 2018. Fatigue strength assessment of duplex and super-duplex stainless steels by 4R method. In: Welding in the World, 62: 6. Pp. 1285–1300.

Carvill, J. 1994. 1.3.4 Stress concentration factors. In: Mechnaical Engineer's Data Handbook. [Referred 9.3.2020] Available: https://www.sciencedirect.com/topics/engineering/stress-concentration-factor

Gurney, T.R. 1979. Fatigue of welded structures. 2nd Edition. Cambridge England: Press Syndicate of the University of Cambridge. 456 p.

Hobbacher, A.F. 2016. Recommendations for Fatigue Design of Welded Joints and Components. 2nd Edition. International Institute of Welding. 143 p.

ISO 5817. 2014. Welding – Fusion-welded joints in steel, nickel, titanium and their alloys (beam welding excluded) – Quality levels for imperfections. 3rd edition. Brussels: European Committee for Standardization. 40 p.

Niemi, E. 1995. Stress Determination for Fatigue Analysis of Welded Components. Cambridge England: Abington Publishing. 80 p.

Nykänen, T. & Björk, T. 2015. A new proposal for assessment of the fatigue strength of steel butt-welded joints improved by peening (HFMI) under constant amplitude tensile loading. Wiley Publishing Ltd. Fatigue Fract Engng Mater Struct., 2016, 39. p. 566-582.

Punkkinen, L. 2019. 2D-tasotapaukset soveltaminen 3D-geometriaan tehollisen lovijännityksen menetelmällä. Batchelor's thesis. Lappeenranta-Lahti University of Technology LUT. 45 p.

Radaj, D., Sonsino, C.M. & Fricke, W. 2006. Fatigue assessment of welded joints by local approaches. 2nd Edition. Cambridge England: Woodhead Publishing Limited. 639 p.

Strain Gauge: Principle, Types, Features and Applications. 2019. [Medium webpage]. Updated July 4, 2019. [Referred 16.3.2020]. Available: https://medium.com/@encardio/strain-gauge-principle-types-features-and-applications-357f6fed86a5

Stress Concentration Factors for Shafts and Cylinders. 2020. [Engineers Edge webpage]. Updated March 9, 2020. [Referred 9.3.2020]. Available: https://www.engineersedge.com/material_science/stress_concentration_factors_14174.htm

Woodford, C. 2019. How strain gauges work [web document]. Updated 27.2.2019. [Referred 16.3.2019]. Available: https://www.explainthatstuff.com/straingauge.html

Window, A.L. & Holister, G.S. 1982. Strain gauge technology. Elsevier Science Publishing CO., INC. 356 p.

APPENDIX I

Weld toe measurements, part 1.

				Weld toe radius *r* [mm]			
	Type	Material	a-measurement	Weld 1	Weld 2	Weld 3	Weld 4
HRO_A_1	BW	S700MC	9,04	5,34	3,83	0,95	1,49
HRO_A_2	BW	S700MC	9,00	14,10	4,10	1,23	5,63
HRO_A_3	BW	S700MC	9,74	11,89	5,51	0,48	0,53
HRO_A_4	BW	S700MC	8,85	5,12	10,98	10,87	1,27
HRO_A_5	BW	S700MC	9,15	13,29	5,60	1,13	4,97
HRO_B_1	LCX	S235	5,26	1,59	1,73	1,97	1,85
HRO_B_2	LCX	S235	5,08	1,27	2,03	1,64	1,66
HRO_B_3	LCX	S235	5,27	2,47	1,47	2,55	1,82
HRO_B_4	LCX	S235	6,33	2,48	0,64	3,13	1,13
HRO_B_5	LG	S700MC	5,82	1,15	-	-	-
HRO_B_6	LG	S700MC	5,91	1,32	-	-	-
HRO_B_7	LG	S700MC	4,58	0,78	-	-	-
HRO_B_8	LG	S700MC	4,62	0,98	-	-	-
HRO_C_1	LCX	S355	3,55	0,99	2,07	3,53	2,79
HRO_C_2	LCX	S355	3,43	2,98	3,04	3,16	1,16
HRO_C_3	LCX	S355	3,56	1,30	1,84	1,45	1,74
HRO_C_4	LCX	S355	3,89	1,14	1,02	2,28	3,05
HRO_C_5	LG	S700MC	5,42	1,45	-	-	-
HRO_C_6	LG	S700MC	5,05	1,70	-	-	-
HRO_C_7	LG	S700MC	5,21	1,02	-	-	-
HRO_C_8	LG	S700MC	5,75	0,88	-	-	-
HRO_D_1	LG	SDX 2507	4,72	0,95	-	-	-
HRO_D_2	LG	SDX 2507	4,88	0,85	-	-	-
HRO_D_3	LG	SDX 2507	4,75	0,96	-	-	-
HRO_D_4	LG	SDX 2507	4,43	1,26	-	-	-
HRO_D_5	LG	S700MC	4,63	1,68	-	-	-
HRO_D_6	LG	S700MC	4,99	1,12	-	-	-
HRO_D_7	LG	S700MC	4,63	1,30	-	-	-
HRO_D_8	LG	S700MC	3,53	0,82	-	-	-

APPENDIX II

Weld toe measurements, part 2.

		Membrane	Bending	Angular	Weld angle β [°]			
	Type	stress $\Delta\sigma_m$	stress $\Delta\sigma_b$	error [°]	Weld 1	Weld 2	Weld 3	Weld 4
HRO_A_1	BW	450	135	1	171,6	165,83	174,62	159,18
HRO_A_2	BW	412,5	140,25	1,5	169,7	166,46	175,08	174,19
HRO_A_3	BW	375	18,75	1	172,59	174,44	121,59	126,23
HRO_A_4	BW	450	85,5	0,5	170,67	172,16	170	173
HRO_A_5	BW	412,5	20,63	3	171,25	169,66	160,29	170,15
HRO_B_1	LCX	142,73	82,79	1,5	136,04	142,21	136,66	139,9
HRO_B_2	LCX	105,88	0	1	132,87	143,59	136,45	141,72
HRO_B_3	LCX	154,88	37,17	2	135,47	130,23	140,28	143,42
HRO_B_4	LCX	210	58,8	1	135,75	131,26	142,18	143,11
HRO_B_5	LG	182,81	51,19	0,5	154,45	-	-	-
HRO_B_6	LG	187,5	48,75	2	158,84	-	-	-
HRO_B_7	LG	154,69	23,2	1,5	158,91	-	-	-
HRO_B_8	LG	156,25	37,5	0,5	162,42	-	-	-
HRO_C_1	LCX	181,37	23,58	3	133,2	143,61	147,22	145,39
HRO_C_2	LCX	162,5	22,75	4	141,34	147,7	150,44	138,26
HRO_C_3	LCX	178,86	25,04	0	139,89	142,27	136,7	146,022
HRO_C_4	LCX	200	26	4,5	138,96	144,12	144,34	147,66
HRO_C_5	LG	182,81	53,02	0,5	158,63	-	-	-
HRO_C_6	LG	154,69	41,77	0	155,42	-	-	-
HRO_C_7	LG	156,25	42,19	0,5	155,58	-	-	-
HRO_C_8	LG	187,5	37,5	1,5	154,61	-	-	-
HRO_D_1	LG	182,81	27,42	0	156,34	-	-	-
HRO_D_2	LG	187,5	39,38	2	154,56	-	-	-
HRO_D_3	LG	210,94	27,42	1,5	154,43	-	-	-
HRO_D_4	LG	210,94	31,64	1	158,09	-	-	-
HRO_D_5	LG	182,81	16,45	0,5	152,32	-	-	-
HRO_D_6	LG	210,94	25,31	1	148,94	-	-	-
HRO_D_7	LG	210,94	33,75	0,5	145,99	-	-	-
HRO_D_8	LG	375	60	1	152,22	-	-	-

APPENDIX III

MathCAD-code for solving unknown 4R variables.

$E := 210000 \qquad h := 1237.5 \qquad n := 0.15$

$\sigma k := 961.4776 \qquad \sigma res := 700$

MAX $\qquad \frac{\sigma max}{E} + \left(\frac{\sigma max}{h}\right)^{\frac{1}{n}} - \frac{(\sigma k + \sigma res)^2}{\sigma max \cdot E}$ solve $\rightarrow 668.48645397377515614$

INPUT MAX AND K $\quad \Delta\sigma k := 480.7388 \qquad \sigma max := 668.48645397378$

$$\frac{\Delta\sigma}{E} + 2\cdot\left(\frac{\Delta\sigma}{2\cdot h}\right)^{\frac{1}{n}} - \frac{(\Delta\sigma k)^2}{\Delta\sigma \cdot E} \text{ solve } \rightarrow 477.15388154298533402$$

INPUT VARIANCE $\quad \Delta\sigma := 477.15388154299$

MIN $\qquad \sigma min := \sigma max - \Delta\sigma = 191.333$

APPENDIX IV

Values used in the calculation of S-N curves, including FAT values at 50 % and 97.7 %.

	n	$y = \log N_f$	$x = \log \Delta\sigma$	k	$\log C_{mean}$	Stdv	FAT 50 %	FAT 97.7 %
Butt	5	25.816	13.111	-5.816	20.414	0.213	267.074	218.475
LCX	16	87.210	36.210	-0.954	7.609	0.210	23.511	8.296
LG	8	43.249	18.072	-3.515	13.348	0.302	101.036	65.006

APPENDIX V

Test results / calculated values -ratio of the fatigue life results.

	Nom. 97.7 %	Nom. 50 %	Hot Spot 97.7 %	Hot Spot 50 %	ENS 97.7 %	ENS 50 %	4R 97.7 %	4R 50 %	Ahola 4R 50 %
HRO_A_1	12.1184	4.7128	11.6840	4.5439	3.0355	1.1805	6.6540	1.1563	0.89446
HRO_A_2	15.9917	6.2192	10.0788	3.9196	1.7314	0.6733	3.8489	0.6689	0.63387
HRO_A_3	15.9287	6.1947	17.5026	6.8068	5.5838	2.1715	9.3758	1.6293	1.63023
HRO_A_4	18.9245	7.3597	18.4464	7.1738	4.4693	1.7381	9.6859	1.6832	1.39479
HRO_A_5	4.3702	1.6996	4.7620	1.8519	1.4520	0.5647	2.0852	0.3624	0.35557
HRO_B_1	23.1350	8.9972	-	-	3.7910	1.4743	-	-	-
HRO_B_2	7.1600	2.7845	-	-	1.1165	0.4342	-	-	-
HRO_B_3	5.4158	2.1062	-	-	1.8116	0.7045	-	-	-
HRO_B_4	10.9665	0.7958	2.9992	1.1664	1.7753	0.6904	0.6556	0.1139	0.14995
HRO_B_5	4.3132	1.6774	10.1808	3.9593	1.4439	0.5615	3.5877	0.6235	0.68156
HRO_B_6	2.9121	1.1325	6.4465	2.5071	1.1157	0.4339	2.9815	0.5181	0.53794
HRO_B_7	1.5880	0.6176	4.8927	1.9028	1.4381	0.5593	2.4373	0.4236	0.5252
HRO_B_8	2.6780	1.0415	11.3217	4.4030	2.2578	0.8781	4.7788	0.8305	0.99376
HRO_C_1	14.3496	5.5806	-	-	1.0112	0.3933	-	-	-
HRO_C_2	12.6047	4.9020	14.7646	5.7420	3.8138	1.4832	1.5898	0.2763	0.51552
HRO_C_3	11.5290	4.4836	-	-	1.4543	0.5656	-	-	-
HRO_C_4	4.5805	1.7814	4.9441	1.9227	1.3331	0.5185	0.6791	0.1180	0.18748
HRO_C_5	3.0560	1.1885	6.7259	2.6157	1.0602	0.4123	2.0907	0.3633	0.40893
HRO_C_6	2.8872	1.1228	6.6800	2.5978	1.0864	0.4225	1.9771	0.3436	0.43447
HRO_C_7	2.5077	0.9752	5.8588	2.2785	1.4191	0.5519	2.9243	0.5082	0.57104
HRO_C_8	1.5960	0.6207	6.3041	2.4516	1.4178	0.5514	3.4925	0.6069	0.62259
HRO_D_1	6.0740	2.3622	20.5333	7.9854	4.9947	1.9424	6.1949	1.0765	1.30578
HRO_D_2	5.9243	2.3040	24.3208	9.4584	5.3156	2.0672	10.6375	1.8486	1.96875
HRO_D_3	4.5792	1.7808	15.3973	5.9880	3.6188	1.4074	3.9133	0.6800	0.78443
HRO_D_4	3.8806	1.5092	13.0707	5.0832	2.7144	1.0556	5.4078	0.9398	0.97829
HRO_D_5	3.6496	1.4193	11.1018	4.3175	2.3238	0.9037	2.5115	0.4365	0.57654
HRO_D_6	2.8281	1.0998	9.4486	3.6746	1.9678	0.7653	3.0357	0.5275	0.58206
HRO_D_7	1.7038	0.6626	6.6641	2.5917	1.7887	0.6956	3.3094	0.5751	0.56056
HRO_D_8	2.5733	1.0007	9.1249	3.5487	2.0623	0.8020	5.1497	0.8949	0.93212
Avg.	7.24	2.69	10.55	4.10	2.36	0.92	4.13	0.72	0.76

APPENDIX VI

SCFs for ENS and 4R.

	Type	ENS Membrane	ENS Bending	4R Membrane	4R Bending
HRO_A_1	Butt	1.718	1.215	1.477	1.143
HRO_A_2	Butt	1.216	1.205	1.189	1.178
HRO_A_3	Butt	1.739	1.176	1.584	1.156
HRO_A_4	Butt	1.604	1.396	1.458	1.23
HRO_A_5	Butt	1.71	1.344	1.467	1.198
HRO_B_1	LCX	4.104	2.241	-	-
HRO_B_2	LCX	3.364	2.06	-	-
HRO_B_3	LCX	3.829	2.123	-	-
HRO_B_4	LCX	2.839	2.026	2.136	1.602
HRO_B_5	LG	2.1	2.509	2.013	2.447
HRO_B_6	LG	2.215	2.635	1.975	2.381
HRO_B_7	LG	2.607	3.06	2.27	2.675
HRO_B_8	LG	2.328	2.743	1.996	2.352
HRO_C_1	LCX	2.346	1.812	-	-
HRO_C_2	LCX	2.163	1.676	1.925	1.602
HRO_C_3	LCX	2.865	1.925	-	-
HRO_C_4	LCX	2.151	1.66	1.911	1.55
HRO_C_5	LG	2.157	2.517	1.913	2.268
HRO_C_6	LG	2.199	2.597	1.908	2.467
HRO_C_7	LG	2.505	3.083	2.073	2.613
HRO_C_8	LG	2.443	2.979	2.107	2.583
HRO_D_1	LG	2.519	3.099	2.116	2.607
HRO_D_2	LG	2.497	2.701	2.112	2.372
HRO_D_3	LG	2.528	3.148	1.971	2.7
HRO_D_4	LG	2.398	2.885	2.006	2.56
HRO_D_5	LG	2.448	3.017	1.971	2.446
HRO_D_6	LG	2.442	3.022	2.104	2.649
HRO_D_7	LG	2.669	3.499	2.131	2.797
HRO_D_8	LG	2.403	3.425	2.111	3.439